Double-Λ, twin-Λ, and single-Λ hypernuclear productions for stopped Ξ^- particles in ^{12}C

Taiichi Yamada[1] and Kiyomi Ikeda[2]
[1]*Laboratory of Physics, Kanto Gakuin University, Yokohama 236, Japan*
[2]*Department of Physics, Niigata University, Niigata 950-21, Japan*
(Received 16 June 1997)

The production rates per Ξ via the $^{12}C+\Xi^-$-atomic states are investigated for the ${}^{12}_{\Lambda\Lambda}Be+p$, ${}^{12}_{\Lambda\Lambda}B+n$, ${}^{11}_{\Lambda\Lambda}Be+d$, ${}^{10}_{\Lambda\Lambda}Be+t$, ${}^{9}_{\Lambda\Lambda}Li+\alpha$, ${}^{6}_{\Lambda\Lambda}He+{}^7Li$, ${}^{5}_{\Lambda\Lambda}H+{}^8Be$, ${}^{9}_{\Lambda}Be+{}^{4}_{\Lambda}H$, ${}^{8}_{\Lambda}Li+{}^{5}_{\Lambda}He$, and ${}^{12}_{\Lambda}B+\Lambda$ channels (including their excited channels) within the frame of the doorway double-Λ hypernuclear picture (direct reaction picture). We found that in the stopped Ξ^- reaction (1) the excited double-Λ hypernuclear states for ${}^{12}_{\Lambda\Lambda}B$, ${}^{12}_{\Lambda\Lambda}Be$, and ${}^{11}_{\Lambda\Lambda}Be$ are produced more strongly than other double-Λ hypernuclei, and (2) the production rates per Ξ depend considerably on the atomic orbital angular momentum of the Ξ^- particle absorbed into nuclei. The calculated production rates per Ξ are discussed in comparison with the KEK-E176 experimental data.
[S0556-2813(97)00412-3]

PACS number(s): 25.80.Pw, 21.80.+a, 21.60.Gx, 27.20.+n

I. INTRODUCTION

One of the important subjects in hypernuclear physics is to study the spectroscopy of the strangeness $S=-2$ hypernuclei. The study of $S=-2$ hypernuclei should lead to the entrance for the structure study of multistrange hadronic systems, and provide interesting information on the unified description of baryon-baryon interactions among the baryon octet, since all the hyperon (Y)-nucleon (N) and Y-Y interactions among the baryon octet are active in the $S=-2$ hypernuclei [1].

The Ξ^--atomic capture reaction at rest in emulsion together with the (K^-,K^+) reaction is a good tool to search double-Λ hypernuclei. The double-Λ hypernuclei are produced via Ξ^--atomic and/or Ξ-hypernuclear states by the elementary process of $\Xi^-+p\rightarrow\Lambda+\Lambda+28$ MeV. According to the recent emulsion-counter hybrid experiment of KEK-E176 [2,3], two kinds of interesting findings have been reported; one is the observation of a double-Λ hypernucleus (one event) [2], and another is twin-Λ hypernuclear production (two events) [3]. The double-Λ hypernucleus is interpreted to ${}^{13}_{\Lambda\Lambda}B$, produced by the sequential decay processes of $({}^{14}N,\Xi^-)_{\rm atom}\rightarrow{}^{14}_{\Lambda\Lambda}C^*+n\rightarrow{}^{13}_{\Lambda\Lambda}B+p+n$, [4] in which the Λ-Λ interaction energy ($\Delta B_{\Lambda\Lambda}=4.9$ MeV) is attractive and is consistent with the old emulsion data (${}^{6}_{\Lambda\Lambda}He$ and ${}^{10}_{\Lambda\Lambda}Be$) [5,6]. It is noted that another experimental interpretation for the observed double-Λ hypernucleus is possible, ${}^{10}_{\Lambda\Lambda}Be$ with $\Delta B_{\Lambda\Lambda}=-4.9$ MeV (repulsive) [2]. However, the theoretical study suggests that the ${}^{13}_{\Lambda\Lambda}B$ hypernucleus is favorable rather than ${}^{10}_{\Lambda\Lambda}Be$ [7]. On the other hand, the twin-Λ hypernuclear production events are found by the following process, $({}^{12}C,\Xi^-)_{\rm atom}\rightarrow{}^{9}_{\Lambda}Be(0^+)+{}^{4}_{\Lambda}H$ and ${}^{9}_{\Lambda}Be^*(2^+)+{}^{4}_{\Lambda}H$, and the experimental analysis showed that both the two events occurred from the Ξ^--atomic states with the binding energy of $B_\Xi\simeq 0.5$ MeV [3].

Three pictures have been proposed so far for the production mechanism of double-Λ and twin-Λ hypernuclei in the Ξ^- capture reaction: First is the quasideuteron model [8], in which a Ξ^- particle in an atomic orbit or a hypernuclear state is absorbed into a quasideuteron in the nucleus to produce a ΛΛ pair (which is trapped to nucleus) and high-energy neutron (which is emitted from nucleus), ''d'' $+\Xi^-\rightarrow$''ΛΛ''$+n$, so that a double-Λ hypernucleus is formed. This picture is able to explain the production of double-Λ hypernuclei. However, it is difficult to describe the twin-Λ hypernuclear production, because a high-energy neutron emission does not accompany the production. The second picture is the compound double-Λ hypernuclear picture, [9] and a third picture is the doorway double-Λ hypernuclear picture (direct reaction picture), which was proposed by the present authors [10]. The difference between the two pictures is given as follows: A Ξ^- particle in an atomic orbit or a hypernuclear state interacts with a proton in nucleus to produce two Λ particles, and then a highly excited double-Λ hypernuclear state $[{}^{A-1}(Z-1)\oplus\Lambda\oplus\Lambda]$ (with the excitation energy of $E_x\simeq 40$ MeV in the case of the $^{12}C+\Xi^-$ atomic system) is formed as an intermediate state with the configuration of two Λ particles coupled with proton-hole core. The highly excited double-Λ hypernuclear state is fragmented to double-Λ hypernucleus or single-Λ hypernucleus by emitting some nucleons or clusters:

$$\begin{aligned}({}^{A}Z,\Xi^-)_{\rm atom}&\rightarrow[{}^{A-1}(Z-1)\otimes\Lambda\otimes\Lambda]\\&\rightarrow[({}^{A_1}Z_1+{}^{A_2}Z_2)\otimes\Lambda\otimes\Lambda]\rightarrow{}^{A_1+2}_{\Lambda\Lambda}Z_1+{}^{A_2}Z_2,\\&\quad{}^{A_1+1}_{\Lambda}Z_1+{}^{A_2+1}_{\Lambda}Z_2,\quad{}^{A}_{\Lambda}(Z-1)+\Lambda,\quad\text{etc.}\quad(1)\end{aligned}$$

where $A_1+A_2=A-1$ and $Z_1+Z_2=Z-1$. The compound double-Λ hypernuclear picture claims that the highly excited double-Λ hypernuclear state is fragmented mainly in the compound-nuclear stage (statistical fragmentation), while the doorway double-Λ hypernuclear picture insists that the highly excited double-Λ hypernuclear state is fragmented mainly in the doorway stage. Therefore, in the compound double-Λ hypernuclear picture, the production rates per Ξ for double-Λ and single-Λ hypernuclei depend mainly on their Q values measured from the ${}^{A}Z+\Xi^-$ threshold, namely, that the final Λ-hypernuclear channel [see Eq. (1)] with the larger Q value has the larger production rate per Ξ. On the other hand, in the doorway double-Λ hypernuclear

picture, the following dynamical factors play an important role in getting the production rates per Ξ large; (1) the spectroscopic factor for the fragmentation of the *proton-hole* state $^{A-1}(Z-1)$ to the $^{A_1}Z_1+^{A_2}Z_2$ channel (if the spectroscopic factor is large, the production rates per Ξ for such channels as $^{A_1+2}_{\Lambda\Lambda}Z_1+^{A_2}Z_2$ and $^{A_2+2}_{\Lambda\Lambda}Z_2+^{A_1}Z_1$ become generally large), and (2) whether the final Λ-hypernuclear channel such as $^{A_1+2}_{\Lambda\Lambda}Z_1+^{A_2}Z_2$ and $^{A_1+1}_{\Lambda}Z_1+^{A_2+1}_{\Lambda}Z_2$ has resonant states around the $^{A}Z+\Xi^-$ threshold or not (if there appear resonant states, the production rate per Ξ becomes large). Since both the doorway process and compound process should contribute in the actual situation, it is important to study the hypernuclear production mechanism in the Ξ^- capture reaction from both the doorway double-Λ hypernuclear picture and compound double-Λ hypernuclear picture.

The purposes of this paper are given as follows. The first is to investigate the production rates per Ξ for double-Λ and twin-Λ hypernuclei via Ξ^--atomic capture reaction in ^{12}C (which is a typical reaction in *p*-shell hypernuclei) within the framework of the doorway double-Λ hypernuclear picture [10]. The second purpose is to clarify the characteristic of the double-Λ and single-Λ hypernuclear productions via the Ξ^--atomic capture, especially, $(3d)_\Xi$- and $(2p)_\Xi$-atomic captures. It is noted that the KEK-E176 experimental results [2,3] and the cascade calculation [11] suggest the Ξ^- particles absorbed mainly from the $(3d)_\Xi$-atomic orbit as well as $(2p)_\Xi$.

Figure 1 shows the various thresholds for double-Λ and single-Λ hypernuclear production channels in the $^{12}C+\Xi^-$ system, in which the energy is measured from the $^{12}C+\Xi^-$ threshold. We see that many production channels are open between the $^{13}_{\Lambda\Lambda}$B ground state and $^{12}C+\Xi^-$ threshold. The double-Λ hypernuclear production channel with the largest Q value is the $^{12}_{\Lambda\Lambda}$Be$+p$ channel ($Q=26.2$ MeV), which is almost degenerate in energy with the $^{12}_{\Lambda\Lambda}$B$+n$ channel ($Q=26.0$ MeV). The Q values for other double-Λ hypernuclear production channels are given as follows; $Q(^{9}_{\Lambda\Lambda}\mathrm{Li}+\alpha)=22.8$ MeV, $Q(^{11}_{\Lambda\Lambda}\mathrm{Be}+d)=19.4$ MeV, $Q(^{10}_{\Lambda\Lambda}\mathrm{Be}+t)=19.2$ MeV, $Q(^{6}_{\Lambda\Lambda}\mathrm{He}+^{7}\mathrm{Li})=15.0$ MeV, $Q(^{10}_{\Lambda\Lambda}\mathrm{Be}+d+n)=17.0$ MeV and $Q(^{5}_{\Lambda\Lambda}\mathrm{H}+^{8}\mathrm{Be})=8.7$ MeV. It is noted that the binding energies for the unknown double-Λ hypernuclei ($^{12}_{\Lambda\Lambda}$B, $^{12}_{\Lambda\Lambda}$Be, $^{11}_{\Lambda\Lambda}$Be, $^{9}_{\Lambda\Lambda}$Li, and $^{5}_{\Lambda\Lambda}$H) are referred from the theoretical analyses (see Sec. III), in which the Λ-Λ interaction is used so as to reproduce the experimental Λ-Λ binding energies of $^{6}_{\Lambda\Lambda}$He, $^{10}_{\Lambda\Lambda}$Be, and $^{13}_{\Lambda\Lambda}$B. On the other hand, there appear only three channels for the twin-Λ hypernuclear production, $^{8}_{\Lambda}$Li$+^{5}_{\Lambda}$He ($Q=13.6$ MeV), $^{9}_{\Lambda}$Be$+^{4}_{\Lambda}$H ($Q=10.0$ MeV) and $^{10}_{\Lambda}$Be$+^{3}_{\Lambda}$H ($Q=6.0$ MeV), and their Q values are generally smaller than those for the double-Λ hypernuclear channels. For the single-Λ hypernuclear production channel, the $^{12}_{\Lambda}$B$+\Lambda$ channel is the largest Q-value channel ($Q=23.9$ MeV), which appears below the $^{9}_{\Lambda\Lambda}$Li$+\alpha$ channel.

In the present paper, we show the production rates per Ξ particle for the following seven double-Λ hypernuclear channels, two twin-Λ hypernuclear channels and one single-Λ hypernuclear channel, including their excited channels: $^{12}_{\Lambda\Lambda}$Be$+p$, $^{12}_{\Lambda\Lambda}$B$+n$, $^{9}_{\Lambda\Lambda}$Li$+\alpha$, $^{11}_{\Lambda\Lambda}$Be$+d$, $^{10}_{\Lambda\Lambda}$Be$+t$, $^{6}_{\Lambda\Lambda}$He$+^{7}$Li, $^{5}_{\Lambda\Lambda}$H$+^{8}$Be, $^{8}_{\Lambda}$Li$+^{5}_{\Lambda}$He, $^{9}_{\Lambda}$Be$+^{4}_{\Lambda}$H, and $^{12}_{\Lambda}$B$+\Lambda$. Their production rates per Ξ are evaluated with use of the distorted-wave impulse approximation (DWIA). Since it is well known that the SU(3)($\lambda\mu$)-state classification is very good to describe the structure of light normal nuclei [12], we employ the SU(3)($\lambda\mu$) wave functions for the nuclear-core parts of single-Λ and double-Λ hypernuclei. The single-Λ and double-Λ hypernuclear wave functions are obtained within the frame of the core$+\Lambda$ and core$+\Lambda+\Lambda$ models, respectively.

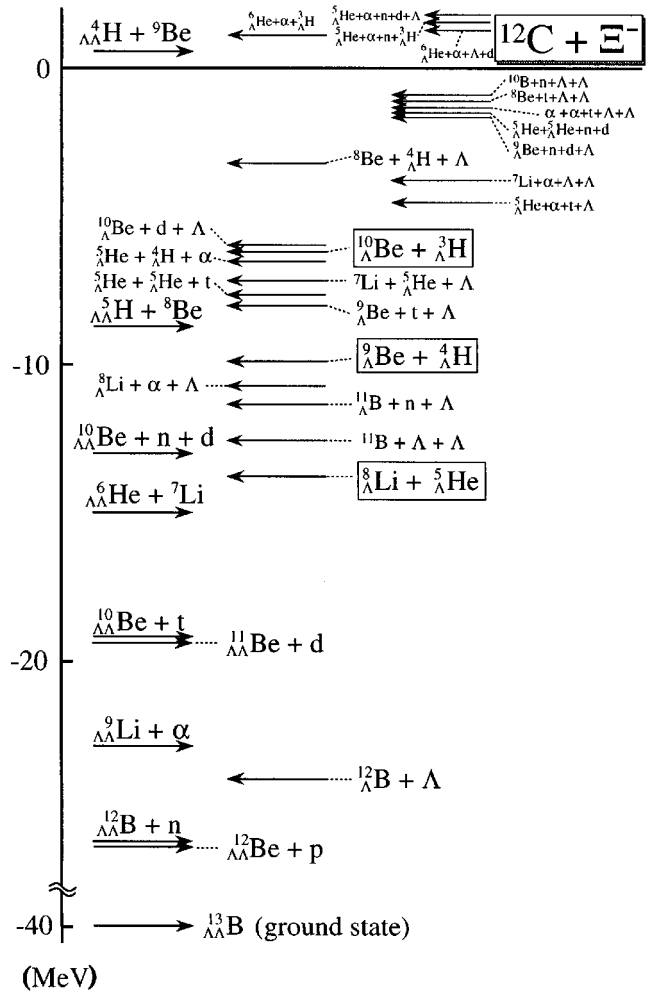

FIG. 1. Various thresholds for double-Λ and single-Λ hypernuclear production channels in the $^{12}C+\Xi^-$ system. The energy is measured from the $^{12}C+\Xi^-$ threshold.

The construction of this paper is as follows. Section II is devoted to the formulation of the production rates per Ξ for double-Λ and single-Λ hypernuclei via Ξ^--atomic states with the use of the DWIA. The double-Λ and single-Λ hypernuclear wave functions needed to calculate the production rates are discussed in Sec. III. The calculated results of the production rates per Ξ for double-Λ, twin-Λ, and single-Λ hypernuclei via Ξ^--atomic orbits are given in Sec. IV, together with the comparison with the KEK-E176 experimental data [2,3]. Finally, we present a summary in Sec. V.

II. FORMULATION

The hypernuclear production rates for the following reactions at rest:

$$({}^{A}Z,\Xi^{-})_{\rm atom}\rightarrow {}^{A_1+2}_{\Lambda\Lambda}Z_1+{}^{A_2}Z_2,$$

$${}^{A_1+1}_{\Lambda}Z_1+{}^{A_2+1}_{\Lambda}Z_2, \quad \text{and} \quad {}^{A'+1}_{\Lambda}Z'+\Lambda, \tag{2}$$

are formulated within the framework of the doorway double-Λ hypernuclear picture. (Here, $A_1+A_2=A-1=A'$ and $Z_1+Z_2=Z-1=Z'$.) We make the distorted-wave impulse approximation (DWIA) to obtain the T matrix for the stopped Ξ^- reaction.

The production width for the reaction shown in Eq. (1), $({}^{A}Z,\Xi^{-})_{\rm atom}\rightarrow C_1+C_2$, with $(C_1,C_2)=({}^{A_1+2}_{\Lambda\Lambda}Z_1,{}^{A_2}Z_2)$, $({}^{A_1+1}_{\Lambda}Z_1,{}^{A_2+1}_{\Lambda}Z_2)$ and $({}^{A'+1}_{\Lambda}Z',\Lambda)$, is presented with the use of the Fermi's golden rule,

$$\Gamma_{fi}=\frac{2\pi}{\hbar}\int\frac{d\mathbf{k}_f}{(2\pi)^3}\,\delta(E_f-E_i)\langle|T_{fi}(\mathbf{k_f})|^2\rangle, \tag{3}$$

$$=\frac{2\pi}{\hbar}\frac{1}{(2\pi)^3}\frac{k_f\omega_f}{\hbar^2}\int d\Omega_{k_f}\langle|T_{fi}(\mathbf{k_f})|^2\rangle, \tag{4}$$

where $\langle\cdots\rangle$ denotes the average over the magnetic quantum numbers of the initial state and the sum over those in the final state for the square of T matrix. The wave number vector $\mathbf{k}_f$ referring to the relative momentum between C_1 and C_2 in the final channel is determined by the energy-conserving δ function, and ω_f is the relative mass energy for the C_1 and C_2 system.

The elementary process for the reaction in Eq. (1) is

$$\Xi^-+p\rightarrow\Lambda+\Lambda, \tag{5}$$

and the conversion process is assumed to be of the ${}^1S_0$-wave type (spin $S=0$ and isospin $T=0$) in this paper. With use of the DWIA, the many-body T matrix in Eq. (4) is given, with the one-body T matrix for the elementary process [Eq. (5)] denoted by t,

$$T_{fi}(\mathbf{k}_f)=\sum_{j=1}^{Z}\langle\Phi_f(\mathbf{k}_f)|t_j|\Phi_i\rangle=t(k_f)\rho_{fi}^{\rm DW}(\mathbf{k}_f), \tag{6}$$

$$\rho_{fi}^{\rm DW}(\mathbf{k}_f)=\langle\Phi_f(\mathbf{k}_f)|\sum_{j=1}^{Z}\delta(\mathbf{r}_j-\mathbf{r}_\Xi)\times[a_\Lambda^+a_\Lambda^+]^{S=T=0}[a_p(j)a_{\Xi^-}]^{S=T=0}|\Phi_i\rangle, \tag{7}$$

where $a_p(j)$ denotes the annihilation operator for the jth proton in the target nucleus, and a_{Ξ^-} and a_Λ^+ represent, respectively, the Ξ^--particle annihilation operator and the Λ-particle creation operator. The vectors $\mathbf{r}_j$ and $\mathbf{r}_\Xi$ are, respectively, coordinates for the jth proton and Ξ^- particle measured from the center-of-mass coordinate of the total system, and the integral for Eqs. (6) and (7) is taken over all the baryon coordinates.

The in-medium two-body production width for the reaction at rest given in Eq. (4) is expressed as

$$\overline{\gamma}=\frac{\overline{k_f}\,\overline{\omega_f}}{\pi\hbar^3}\,|t(\overline{k_f})|^2, \tag{8}$$

where $\overline{k_f}$ and $\overline{\omega_f}$ are the Fermi-averaged in-medium quantities for the wave number and energy of the Λ particle. Then, the production width in Eq. (3) is expressed as

$$\Gamma_{fi}=\frac{k_f\omega_f}{\overline{k_f}\,\overline{\omega_f}}\,\overline{\gamma}\int d\Omega_{k_f}\langle|\rho_{fi}^{\rm DW}(\mathbf{k_f})|^2\rangle/4\pi. \tag{9}$$

It is found that the Fermi-averaged in-medium quantities $\overline{k_f}$ and $\overline{\omega_f}$ do not change seriously from the elementary-process quantities. (Their differences are within about 10%.) In the present study, we use the following values for $\overline{k_f}$ and $\overline{\omega_f}$; $\overline{k_f}=0.909$ fm^{-1} and $\overline{\omega_f}=1130$ MeV.

The wave function of the initial state given in Eq. (6) is expressed as

$$\Phi_i=\Phi_{I_cM_cT_ct_c}({}^{A}Z)\chi_{n_\Xi l_\Xi m_\Xi}(\mathbf{r}_\Xi), \tag{10}$$

where $\Phi_{I_cM_cT_ct_c}({}^{A}Z)$ and $\chi_{n_\Xi l_\Xi j_\Xi m_\Xi}$ denote the target wave function with the angular momentum I_c (the magnetic quantum number M_c) and isospin T_c (the z component t_c), and the Ξ^--atomic wave function with the principal number n_Ξ and the orbital angular momentum l_Ξ (the magnetic quantum number m_Ξ), respectively. In the present paper, we use the SU(3)$[f](\lambda\mu)=[444](04)$ wave function for the ^{12}C ground-state wave function ($I_c=T_c=0$) for simplicity, whose rms of radius is fitted to the experimental value. It should be noted that the SU(3)$[f](\lambda\mu)=[444](04)$ eigenstate is a main component of the ^{12}C ground-state wave function, according to the microscopic-cluster-model and shell-model analyses. For convenience of the practical calculation, the $[444](04)$ wave function of ^{12}C is decomposed as

$$\Phi({}^{12}\mathrm{C}[444](04);0^+)=c(0s)[\Phi({}^{11}\mathrm{B}[443](04);0^+)\otimes\phi_p(0s)]_{0^+}+c(0p)[\Phi({}^{11}\mathrm{B}[443](13);1^-)\otimes\phi_p(0p)]_{0^+}, \tag{11}$$

where $c(0s)$ ($c(0p)$) are the expansion coefficients, and $\Phi({}^{11}\mathrm{B}[443](04);0^+)$ [$\Phi({}^{11}\mathrm{B}[443](31);1^-)$] and $\phi(0s)$ ($\phi_p(0p)$) represent, respectively, the SU(3)$[f](\lambda\mu)=[443](04)$ ($[443](31)$) wave function of ^{11}B and proton wave function in the $0s$ ($0p$) orbit. It is noted here that the SU(3)$[f](\lambda\mu)=[443](04)$ ($[443](31)$) state of ^{11}B corresponds to the s-hole (p-hole) state of ^{11}B [13]. In the calculation of $\rho_{fi}^{\rm DW}(\mathbf{k_f})$ in Eq. (9), we need the spectroscopic amplitudes for the fragmentation of the ^{11}B(s-hole) and ^{11}B(p-hole) states to the ${}^{A_1}Z_1$ and ${}^{A_2}Z_2$ channel. As will be given in Sec. III, the ${}^{A_1}Z_1$ and ${}^{A_2}Z_2$ nuclei are described by the SU(3)$[f](\lambda\mu)$ wave functions. Therefore, the spectroscopic amplitudes obtained by the SU(3)$[f](\lambda\mu)$ wave functions are employed in the present calculation.

For the Ξ^--atomic wave function, we solve the Schrödinger equation with the uniform-charged Coulomb potential and the Ξ-nucleus potential $V_\Xi(R)$ [1] expressed by

$$V_\Xi(R)=-\frac{V_{0\Xi}}{1+\exp[(R-R_A)/a]}, \tag{12}$$

$$R_A=R_0A^{1/3}, \quad R_0=1.2\ \text{fm}. \tag{13}$$

In the present study, the strength $V_{0\Xi}$ in Eq. (12) is treated as a real quantity not a complex quantity. The reason is given as follows: The imaginary part of the Ξ-nucleus optical potential which gives the total width of the relevant Ξ^--atomic system comes mainly from the elementary process of $\Xi^-+p\rightarrow\Lambda+\Lambda+28$ MeV. Since the elementary process causes

various Λ-hypernuclear productions shown in Fig. 1, the total width of the Ξ^--atomic system is presented mainly as a sum over partial production widths for various Λ-hypernuclear production channels, whose quantities are calculated in the present paper. Therefore, the imaginary part of the Ξ-nucleus optical potential which simulates various Λ-hypernuclear production processes is not required in the present framework. This treatment, of course, is based on an assumption of a relatively low strength of the $\Xi^- + p \to \Lambda + \Lambda$ process. The assumption is supported by the theoretical studies [1,14] based on the Nijmegen one boson exchange potentials [15]. Since the strength $V_{0\Xi}$ in Eq. (12) is unknown experimentally, we study the dependence of the partial production widths (Γ_{fi}) and production rates per Ξ (R_{fi}) on the strength $V_{0\Xi}$.

The final-state continuum wave function adopted in Eq. (6) is described within the frame of the microscopic cluster model and expressed as

$$\Phi_f(\mathbf{k}_f) = \sqrt{\frac{A_1!A_2!}{(A_1+A_2)!}} \times \mathcal{A}'\{[\phi_{I_1T_1}(C_1)\phi_{I_2T_2}(C_2)]_{I_fM_fT_ft_f}\varphi_{\mathbf{k_f}}(\mathbf{R})\}, \tag{14}$$

where $\phi_{I_1T_1}(C_1)$ $[\phi_{I_2T_2}(C_2)]$ denotes the intrinsic wave function of the C_1 (C_2) cluster with the angular momentum I_1 (I_2) and isospin T_1 (T_2), for which the explicit expression is shown in Sec. III. The operator $\mathcal{A}'$ antisymmetrizes nucleons belonging to different clusters as well as two Λ particles. The wave function $\varphi_{\mathbf{k_f}}(\mathbf{R})$ with respect to the relative coordinate $\mathbf{R}$ between the C_1 and C_2 clusters is given in terms of the partial-wave expansion

$$\varphi_{\mathbf{k_f}}(\mathbf{R}) = \sum_L i^L(2L+1)\varphi_L(k_f,R)P_L(\widehat{\mathbf{k_f}\cdot\mathbf{R}}). \tag{15}$$

The radial wave function φ_L reduces to the spherical Bessel function $j_L(k_fR)$ for the case without the Coulomb and nuclear potentials. The way to obtain the continuum wave function is given in Sec. III.

The total width is defined as the summation over the production widths given in Eq. (9) and presented as

$$\Gamma = \sum_f \Gamma_{fi}, \tag{16}$$

which corresponds to the width of the Ξ^--atomic state coming from the conversion process, $\Xi^- p \to \Lambda\Lambda$. In order to estimate the value of Γ, we use the closure approximation for the summation over all final states, neglecting the k_f dependence of the final states, replacing it by $\overline{k_k}$ and ω_f by $\overline{\omega_f}$ in Eq. (9),

$$\Gamma = \overline{\gamma}\langle\Phi(^{12}C)\chi_\Xi(\mathbf{r})|\sum_{j=1}^{Z}[a_p^+(j)a_{\Xi^-}^+]^{S=T=0}[a_p(j)a_{\Xi^-}]^{S=T=0}|\Phi(^{12}C)\chi_\Xi(\mathbf{r})\rangle. \tag{17}$$

Here, we make the matter approximation for the matrix element in Eq. (17),

$$\Gamma = \overline{\gamma}\frac{1}{16}\langle\Phi(^{12}C)\chi_\Xi(\mathbf{r})|\sum_{(ST)}\sum_{j=1}^{A}[a_N^+(j)a_\Xi^+]^{ST}[a_N(j)a_\Xi]^{ST}|\Phi(^{12}C)\chi_\Xi(\mathbf{r})\rangle, \tag{18}$$

$$= \overline{\gamma}\frac{1}{16}\int d\mathbf{r}\,\rho_C(\mathbf{r})|\chi_\Xi(\mathbf{r})|^2, \tag{19}$$

where a_N and a_Ξ (a_N^+ and a_Ξ^+) are, respectively, the nucleon and Ξ-particle annihilation (creation) operators and the number 16 corresponds to the number of channels for total spin (S) and total isospin (T) in nucleon and Ξ-particle systems. The nucleon density of ^{12}C, $\rho_C(\mathbf{r})$, is normalized as

$$\int d\mathbf{r}\,\rho_C(\mathbf{r}) = 12. \tag{20}$$

Then, the production rate per Ξ particle is defined as

$$R_{fi} = \Gamma_{fi}/\Gamma, \tag{21}$$

which calculated values are discussed in Sec. IV.

III. SINGLE-Λ AND DOUBLE-Λ HYPERNUCLEI

As will be discussed in Sec. IV, we calculate the production rates for the following two-body channels from ^{12}C $+\Xi^-$-atomic states; $^{12}_{\Lambda\Lambda}$Be$+p$, $^{12}_{\Lambda\Lambda}$B$+n$, $^{9}_{\Lambda\Lambda}$Li$+\alpha$, $^{11}_{\Lambda\Lambda}$Be $+d$, $^{10}_{\Lambda\Lambda}$Be$+t$, $^{6}_{\Lambda\Lambda}$He$+^7$Li, $^{5}_{\Lambda\Lambda}$H$+^8$Be, $^{8}_{\Lambda}$Li$+^5_\Lambda$He, $^{9}_{\Lambda}$Be$+^4_\Lambda$H, and $^{12}_{\Lambda}$B$+\Lambda$ channels. For this purpose, the single-Λ and double-Λ hypernuclear wave functions are needed to calculate the production rates.

A. Single-Λ hypernuclear wave function

Concerning the $^4_\Lambda$H, $^5_\Lambda$He, $^8_\Lambda$Li, $^9_\Lambda$Be, and $^{12}_\Lambda$B hypernuclei, the single-Λ wave function with the angular momentum J_Λ and isospin T_Λ is described within the frame of the core $(^AZ)+\Lambda$ model ($t+\Lambda$, $\alpha+\Lambda$, ^{7}Li$+\Lambda$, ^{8}Be$+\Lambda$, and ^{11}B $+\Lambda$, respectively), and is given as

$$\Phi_{J_\Lambda T_\Lambda}(^{A+1}_\Lambda Z) = \sum_{c,n_r} a_c(n_r)\Phi_c(n_r), \tag{22}$$

$$\Phi_c(n_r) = [\Phi_{IT}(^AZ)[u_{n_rl_r}(\mathbf{r})\chi_{s_\Lambda}]_{j_\Lambda}]_{J_\Lambda T_\Lambda}, \tag{23}$$

$$c = (I, l_r, s_\Lambda = 1/2, j_\Lambda, J_\Lambda), \tag{24}$$

with $\mathbf{j}_\Lambda=\mathbf{l}_r+\mathbf{s}_\Lambda$ and $\mathbf{J}_\Lambda=\mathbf{I}+\mathbf{j}_\Lambda$. $a_c(n_r)$ represents the expansion coefficient and, $\Phi_{IT}(^{A_1}Z_1)$ denotes the core-part wave function with the angular momentum I and isospin T. The relative wave function referring to the relative coordinate $\mathbf{r}$ between the core and Λ particle is expanded in terms of the harmonic oscillator wave function $u_{n_r l_r}$ with the relative coordinate angular momentum l_r and node number n_r [see Eq. (23)].

For the t and α nuclei, we use the lowest shell-model wave functions with the $(0s)^3$ and $(0s)^4$ configurations, respectively. The nucleon size parameter b_N is chosen to reproduce the experimental rms of radius ($b_N=1.67$ fm and 1.358 fm for t and α nuclei, respectively). Concerning the ^{7}Li, ^{8}Be, and ^{11}B wave functions, the SU(3)($\lambda\mu$) wave functions are employed as $(\lambda\mu)_{l^\pi}=(30)_{1^-,3^-}$, $(40)_{0^+,2^+,4^+}$ and $(13)_{1^-,2^-,3^-4^-}$, respectively. It should be noted that the SU(3)($\lambda\mu$) classification is very good to describe the structure of light nuclei. Their wave functions are described by the microscopic cluster models, $\alpha+3N$, $\alpha+\alpha$, ^{8}Be$+3N$, respectively, with the nucleon size parameter $b_N=1.48$ fm, where $3N$ denotes the t-^{3}He cluster. For example, the ^{8}Be$(\lambda\mu)=(40)$ and ^{11}B$(\lambda\mu)=(13)$ wave functions are given

$$\Phi_l(^8\mathrm{Be})=\frac{1}{\sqrt{\nu(40)}}\sqrt{\frac{4!4!}{8!}}\,\mathcal{A}'\{\phi_\alpha\phi_\alpha u_{nl}(\mathbf{r_{44}})\}_{2n+l=4}, \tag{25}$$

$$\Phi_{lsjt}(^{11}\mathrm{B})=\frac{1}{\sqrt{\nu(13)}}\sum_{l_{44},n_{83}l_{83}} a^{lsjt}_{l_{44},n_{83}l_{83}}\Phi_{lsjt}(l_{44},n_{83},l_{83}), \tag{26}$$

$$\Phi_{lsjt}(l_{44},n_{83}l_{83})=\sqrt{\frac{8!3!}{10!}}\,\mathcal{A}'\{\phi_{3N}(s,t)\times[\Phi_{l_{44}}(^8\mathrm{Be})u_{n_{83}l_{83}}(\mathbf{r_{83}})]_l\}_{jt}, \tag{27}$$

with $\mathbf{l}=\mathbf{l}_{44}+\mathbf{l}_{83}$ and $2n_{83}+l_{83}=3$. The internal wave functions, ϕ_α and ϕ_t, are given as the lowest shell-model wave functions with the $(0s)^4$ and $(0s)^3$ configurations, respectively. The operator $\mathcal{A}'$ antisymmetrizes nucleons belonging to different clusters. The relative wave function referring to the relative coordinate $\mathbf{r_{44}}$ ($\mathbf{r_{83}}$) between the α and α clusters (^{8}Be and t) is expanded in terms of the harmonic oscillator wave function $u_{n_{44}l_{44}}$ ($u_{n_{83}l_{83}}$) with the relative orbital angular momentum l_{44} (l_{83}) and node number n_{44} (n_{83}). The expansion coefficient $a^{lsjt}_{l_{44},n_{83}l_{83}}$ and eigenvalue $\nu(13)$ in Eq. (26) are obtained by diagonalization of the norm kernel matrix on the basis of $\Phi_{lsjt}(l_{44},n_{83}l_{83})$ given in Eq. (27).

The total Hamiltonian of the core$+\Lambda$ system is given as

$$H_\Lambda=h(\mathrm{core})+T_r+\sum_{i=1}^{A}u_{\Lambda N}(\Lambda;i), \tag{28}$$

where $h(\mathrm{core})$ and T_r denote, respectively, the Hamiltonian of core part and the relative kinetic energy operator. In the present paper, the eigenvalues for the nuclear core states $\langle\Phi_{IT}|h(\mathrm{core})|\Phi_{IT}\rangle$ are replaced by values of the experimental energies averaged with respect to the nuclear spin. Their energies are shown in Table I. The Λ-N interaction $v_{\Lambda N}$ is given by the one-range Gaussian, for simplicity,

$$v_{\Lambda N}(r)=v^0_{\Lambda N}\exp[-(r/\beta_{\Lambda N})^2],\quad \beta_{\Lambda N}=1.034\ \mathrm{fm}, \tag{29}$$

where the range $\beta_{\Lambda N}$ is equivalent to the two-pion exchange Yukawa. The strength $v^0_{\Lambda N}$ is chosen to reproduce the experimental Λ binding energy for the ground state (see Table II). In the case of $^{12}_{\Lambda}$B, we derive the ^{11}B$-\Lambda$ potential from the ^{8}Be$-\Lambda$ and $t-\Lambda$ folding potentials for simplicity. The strength of the ^{11}B$-\Lambda$ potential is adjusted to reproduce the experimental binding energy of the Λ particle in $^{12}_{\Lambda}$B. We neglect the spin-orbit and spin-spin terms of the Λ-N interaction because of their small effects. Therefore, the single-Λ hypernuclear states obtained by the present model are degenerate in energy with respect to the Λ-particle spin and/or core-part spin, and their eigenstates are characterized by the total orbital angular momentum L.

The model space is characterized by the angular momentum channel c and number of nodes n_r [see Eq. (22)]. For $^4_\Lambda$H, $^5_\Lambda$He, $^8_\Lambda$Li, and $^9_\Lambda$Be, the following model space is taken: $l_r=0$ and $n_r=0,1,\ldots 5$. For $^{12}_\Lambda$B, we take $l_r=0,1$ and $n_r=0,1\ldots 5$. The model space is enough to describe the low-lying states of the single-Λ hypernuclei. The Hamiltonian matrix elements on the basis of $\Phi_c(n_r)$ [see Eqs. (23) and (28)] are diagonalized to obtain the eigenenergies and expansion coefficients $a_c(n_r)$ given in Eq. (22). As a result, we found that the effect of the channel coupling among the states of nuclear core part is small. Therefore, in the calculation of the Λ-hypernuclear production rates for the Ξ^--atomic capture reaction, we use the single-Λ hypernuclear wave functions with no channel coupling for simplicity.

TABLE I. Excitation energies for the nuclear-core states of ^{7}Li, ^{8}Be, and ^{11}B. They are obtained from the experimental energies averaged over the nuclear-core spin.

^{7}Li(l^π)	E_x (MeV)	^{8}Be(l^π)	E_x (MeV)	^{11}B(l^π)	E_x (MeV)
1^-	0.0	0^+	0.0	1^-	0.0
3^-	5.8	2^+	2.9	2^-	3.9
		4^+	11.4	3^-	6.8
				4^-	10.3

B. Double-Λ hypernuclear wave function

The double-Λ hypernuclear wave function (the total angular momentum $J_{\Lambda\Lambda}$ and isospin $T_{\Lambda\Lambda}$) for $^{12}_{\Lambda\Lambda}$B, $^{12}_{\Lambda\Lambda}$Be,

TABLE II. Values for the strength $v^0_{\Lambda N}$ of the one-range ΛN interaction. They are determined so as to reproduce the experimental binding energy of the Λ particle within the frame of the $t+\Lambda$, $\alpha+\Lambda$, ^{7}Li$+\Lambda$, and ^{8}Be$+\Lambda$ models, respectively.

	$^4_\Lambda$H	$^5_\Lambda$He	$^8_\Lambda$Li	$^9_\Lambda$Be
$v^0_{\Lambda N}$ (MeV)	-55.80	-38.19	-36.60	-32.85

$^{11}_{\Lambda\Lambda}$Be, $^{10}_{\Lambda\Lambda}$Be, $^{9}_{\Lambda\Lambda}$Li, $^{6}_{\Lambda\Lambda}$He, and $^{5}_{\Lambda\Lambda}$H is described by the core(^AZ)+Λ+Λ model ($^AZ=^{10}$B, ^{10}Be, ^{9}Be, ^{8}Be, ^{7}Li, α, and t, respectively):

$$\Phi_{J_{\Lambda\Lambda}T_{\Lambda\Lambda}}(^{A+2}_{\Lambda\Lambda}Z)=\sum_{c,n_r,n_p} a_c(n_r,n_\rho)\Phi_c(n_r,n_\rho), \quad (30)$$

$$\Phi_c(n_r,n_\rho)=[\Phi_{IT}(^{A_1}Z_1) \times[[u_{n_r l_r}(\mathbf{r})u_{n_\rho l_\rho}(\boldsymbol{\rho})]_{L_{\Lambda\Lambda}}\chi_{S_{\Lambda\Lambda}}]_{I_{\Lambda\Lambda}}]_{J_{\Lambda\Lambda}T_{\Lambda\Lambda}}, \quad (31)$$

$$c=(I,l_r,l_\rho,L_{\Lambda\Lambda},S_{\Lambda\Lambda},I_{\Lambda\Lambda},J_{\Lambda\Lambda}), \quad (32)$$

with $\mathbf{L}_{\Lambda\Lambda}=\mathbf{l}_r+\mathbf{l}_\rho$, $\mathbf{I}_{\Lambda\Lambda}=\mathbf{L}_{\Lambda\Lambda}+\mathbf{S}_{\Lambda\Lambda}$ and $\mathbf{J}_{\Lambda\Lambda}=\mathbf{I}+\mathbf{I}_{\Lambda\Lambda}$. $a_c(n_r,n_\rho)$ represents the expansion coefficient. The relative wave function referring to the relative coordinate $\boldsymbol{\rho}$ ($\mathbf{r}$) between the two Λ particles (the core and center-of-mass of two Λ particles) is expanded in terms of the harmonic oscillator wave function $u_{n_\rho l\rho}$ ($u_{n_r l_r}$) with the relative coordinate angular momentum l_ρ (l_r) and node number n_ρ (n_r). The antisymmetrization between the two Λ particles demands the relation of $l_\rho+S_{\Lambda\Lambda}=$even, where $S_{\Lambda\Lambda}$ denotes the total spin for the two Λ particles.

The total Hamiltonian of the core+Λ+Λ system is given as

$$H_{\Lambda\Lambda}=h(\text{core})+T_r+T_\rho+\sum_{k=1}^{2}\sum_{i=1}^{A} v_{\Lambda N}(\Lambda_k;i)+v_{\Lambda\Lambda}, \quad (33)$$

where T_r (T_ρ) denotes the relative kinetic energy operator referring to the relative coordinate $\mathbf{r}$ ($\boldsymbol{\rho}$), and $v_{\Lambda N}$ ($v_{\Lambda\Lambda}$) represents the Λ-N (Λ-Λ) interaction. In the present paper, the eigenvalues for the nuclear-core states $\langle\Phi_{IT}|h(\text{core})|\Phi_{IT}\rangle$ are replaced by values of the experimental energies averaged with respect to the nuclear-core spin (see Sec. III A). Their energies are shown in Table I. For the Λ-N interaction, we use the one-range Gaussian-type interaction given in Eq. (29). The strength $v^0_{\Lambda N}$ in Eq. (29) is chosen to reproduce the experimental Λ binding energy of the core+Λ system (see Sec. III A). On the other hand, the YNG-D effective interaction [14] is employed for the Λ-Λ interaction, which is obtained by applying the G-matrix theory to the Nijmegen model-D potential [15]. In the present study, only the $^1S_0$-type Λ-Λ interaction is taken into account. The YNG-D Λ-Λ interaction is given as

$$v_{\Lambda\Lambda}(r)=\sum_{k=1}^{3} v^{(k)}_{\Lambda\Lambda}\exp[-(r/\beta^{(k)}_{\Lambda\Lambda})^2], \quad (34)$$

where the ranges and strengths are given in Table III. It is noted that the YNG-D interaction [14] gives the attractive Λ-Λ binding energy, which is consistent with the experimental Λ-Λ binding energy ($\Delta B^{\text{exp}}_{\Lambda\Lambda}\simeq$4–5 MeV) for $^{6}_{\Lambda\Lambda}$He, $^{10}_{\Lambda\Lambda}$Be, and $^{13}_{\Lambda\Lambda}$B [5,6,4].

Concerning the wave function of core part [$\Phi_{IT}(^AZ)$] given in Eq. (31), we use the SU(3)($\lambda\mu$) wave functions, $(\lambda\mu)_{I^\pi}=(13)_{1^-,2^-,3^-,4^-}$ for ^{11}B, $(22)_{0^+,2^+_1,2^+_2,3^+,4^+}$ for ^{10}B, $(22)_{0^+,2^+_1,2^+_2,3^+,4^+}$ for ^{10}Be, $(31)_{1^-,2^-,3^-,4^-}$ for ^{9}Be, $(40)_{0^+,2^+,4^+}$ for ^{8}Be, and $(30)_{1^-,3^-}$ for ^{7}Li, with the nucleon size parameter $b_N=1.48$ fm. They are obtained by the microscopic cluster model technique, within the frame of the microscopic cluster models, ^{8}Be+3N, ^{8}Be+2N, ^{8}Be+2N, ^{8}Be+N, $\alpha+\alpha$ and $\alpha+3N$, respectively (see Sec. III A).

TABLE III. Ranges and strengths of the YNG-ND ΛΛ interaction, Ref. [14].

k	1	2	3
$\beta^{(k)}_{\Lambda\Lambda}$ (fm)	1.5	0.9	0.5
$v^{(k)}_{\Lambda\Lambda}$ (MeV)	−8.951	−223.1	948.9

The model space is characterized by the angular momentum channel c and number of node (n_r,n_ρ) [see Eq. (30)]. Since the elementary conversion process ($\Xi^-+p\rightarrow\Lambda+\Lambda$) is assumed to be of the $^1S_0$ type, the total spin of two Λ particles is fixed to $S_{\Lambda\Lambda}=0$ and $l_\rho=0$. For the $^{5}_{\Lambda\Lambda}$H, $^{6}_{\Lambda\Lambda}$He, $^{9}_{\Lambda\Lambda}$Li, $^{10}_{\Lambda\Lambda}$Be, and $^{11}_{\Lambda\Lambda}$Be hypernuclei, only $(l_r,l_\rho)_{L_{\Lambda\Lambda}}=(0,0)_0$ is taken with $n_r=0,1\ldots5$ and $n_\rho=0,1\ldots5$, for which the model space is enough to describe the low-lying states of the double-Λ hypernuclei. The angular momentum channel $(l_r,l_\rho)_{L_{\Lambda\Lambda}}=(0,0)_0$ means that both the two Λ particles occupy in the $(0s)_\Lambda$ orbit, namely, $(0s)^2_\Lambda$, according to the shell-model terminology. On the other hand, for the $^{12}_{\Lambda\Lambda}$B and $^{12}_{\Lambda\Lambda}$Be hypernuclei, the following model space is taken: $(l_r,l_\rho)_{L_{\Lambda\Lambda}}=(0,0)_0$ and $(1,0)_1$ with $n_r=0,1\ldots5$ and $n_\rho=0,1\ldots5$. The $(l_r,l_\rho)_{L_{\Lambda\Lambda}}=(1,0)_1$ channel is in correspondence with the fact that one of two Λ particles occupies in the $(0s)_\Lambda$ orbit and other in $(0p)_\Lambda$, namely, $(0s)_\Lambda(0p)_\Lambda$, according to the shell-model terminology. Then, we can describe the following double-Λ hypernuclear states;

$^{5}_{\Lambda\Lambda}$H; $L^\pi=0^+$ with $(s,t)=(1/2,1/2)$,

$^{6}_{\Lambda\Lambda}$He; $L^\pi=0^+$ with $(s,t)=(0,0)$,

$^{9}_{\Lambda\Lambda}$Li; $L^\pi=1^-,3^-$ with $(s,t)=(1/2,1/2)$,

$^{10}_{\Lambda\Lambda}$Be; $L^\pi=0^+,2^+,4^+$ with $(s,t)=(0,0)$,

$^{11}_{\Lambda\Lambda}$Be; $L^\pi=1^-,2^-,3^-,4^-$ with $(s,t)=(1/2,1/2)$,

$^{12}_{\Lambda\Lambda}$Be; $L^\pi=0^+,2^+,3^+,4^+,1^-2^-,3^-,4^-,5^-$ with $(s,t)=(0,1)$,

$^{12}_{\Lambda\Lambda}$B; $L^\pi=0^+,2^+,3^+,4^+,1^-,2^-,3^-,4^-,5^-$ with $(s,t)=(0,1)$ and $(1,0)$,

where L denotes the total orbital angular momentum, and s and t represent the nuclear-core part spin and isospin, respectively. The Hamiltonian matrix elements on the basis of $\Phi_c(n_r,n_\rho)$ are diagonalized to obtain the eigenenergies and expansion coefficients $a_c(n_r,n_\rho)$ given in Eq. (30). Since the effect of the channel coupling among the states of the nuclear core part is found to be small, we use the double-Λ hyper-

TABLE IV. Production rates per Ξ^- (R/Ξ^-) for double-Λ and single-Λ hypernuclei in the case of the absorption from the $(2p)_{\Xi^-}$- and $(3d)_{\Xi^-}$-atomic orbits with a Ξ-nucleus potential strength of $V_{0\Xi}=16$ and 24 MeV. Λ_s (Λ_p) denotes the Λ particle in the s (p) state.

		$V_{0\Xi}=16$ MeV		$V_{0\Xi}=24$ MeV	
Channel	Q (MeV)	$(2p)_{\Xi^-}$ (%)	$(3d)_{\Xi^-}$ (%)	$(2p)_{\Xi^-}$ (%)	$(3d)_{\Xi^-}$ (%)
${}^{12}_{\Lambda_s\Lambda_s}\mathrm{B}(0^+)^{t=0s=1}+n$	26.0	0.02	0.02	0.01	0.02
${}^{12}_{\Lambda_s\Lambda_s}\mathrm{B}(2_1^+)^{t=0s=1}+n$	22.6	0.02	0.00	0.02	0.00
${}^{12}_{\Lambda_s\Lambda_s}\mathrm{B}(2_2^+)^{t=0s=1}+n$	14.1	2.28	0.10	1.93	0.10
${}^{12}_{\Lambda_s\Lambda_s}\mathrm{B}(0^+)^{t=1s=0}+n$	24.0	0.01	0.01	0.01	0.01
${}^{12}_{\Lambda_s\Lambda_s}\mathrm{B}(2_1^+)^{t=1s=0}+n$	20.9	0.01	0.00	0.01	0.00
${}^{12}_{\Lambda_s\Lambda_s}\mathrm{B}(2_2^+)^{t=1s=0}+n$	12.4	0.95	0.04	0.80	0.04
${}^{12}_{\Lambda_s\Lambda_p}\mathrm{B}(1_1^-,1_2^-,2^-,3^-)^{t=0s=1}+n$	7.0–11.9	0.49	0.92	0.41	0.91
${}^{12}_{\Lambda_s\Lambda_p}\mathrm{B}(1_1^-,1_2^-,2^-,3^-)^{t=1s=0}+n$	5.0–9.9	0.19	0.39	0.16	0.38
	Sum	3.96%	1.47%	3.35%	1.45%
${}^{12}_{\Lambda_s\Lambda_s}\mathrm{Be}(0^+)+p$	26.2	0.03	0.02	0.03	0.02
${}^{12}_{\Lambda_s\Lambda_s}\mathrm{Be}(2_1^+)+p$	22.8	0.02	0.00	0.02	0.00
${}^{12}_{\Lambda_s\Lambda_s}\mathrm{Be}(2_2^+)+p$	14.3	2.03	0.07	1.71	0.07
${}^{12}_{\Lambda_s\Lambda_p}\mathrm{Be}(1_1^-,1_2^-,2^-,3^-)+p$	7.0–11.9	0.34	0.91	0.31	0.90
	Sum	2.43%	1.00%	2.07%	0.99%
${}^{11}_{\Lambda_s\Lambda_s}\mathrm{Be}(1^-)+d$	19.4	0.12	0.04	0.11	0.03
${}^{11}_{\Lambda_s\Lambda_s}\mathrm{Be}(3^-)+d$	13.5	0.42	0.04	0.36	0.04
${}^{11}_{\Lambda_s\Lambda_p}\mathrm{Be}(0^+)+d$	4.7	0.00	0.30	0.00	0.29
${}^{11}_{\Lambda_s\Lambda_p}\mathrm{Be}(2_1^+)+d$	5.1	0.04	1.68	0.03	1.65
${}^{11}_{\Lambda_s\Lambda_p}\mathrm{Be}(2_2^+)+d$	0.1	0.00	0.00	0.00	0.00
	Sum	0.59%	2.05%	0.50%	2.01%
${}^{10}_{\Lambda_s\Lambda_s}\mathrm{Be}(0^+)+t$	19.2	0.06	0.00	0.05	0.00
${}^{10}_{\Lambda_s\Lambda_s}\mathrm{Be}(2^+)+t$	16.3	0.06	0.00	0.05	0.00
${}^{10}_{\Lambda_s\Lambda_s}\mathrm{Be}(4^+)+t$	7.8	0.02	0.02	0.02	0.02
	Sum	0.14%	0.02%	0.12%	0.02%
${}^{9}_{\Lambda_s\Lambda_s}\mathrm{Li}(1^-)+\alpha$	22.8	0.04	0.00	0.04	0.00
${}^{9}_{\Lambda_s\Lambda_s}\mathrm{Li}(3^-)+\alpha$	17.0	0.01	0.02	0.01	0.02
	Sum	0.05%	0.02%	0.05%	0.02%
${}^{6}_{\Lambda_s\Lambda_s}\mathrm{He}+{}^{7}\mathrm{Li}(1^-)$	15.0	0.02	0.15	0.02	0.15
${}^{6}_{\Lambda_s\Lambda_s}\mathrm{He}+{}^{7}\mathrm{Li}(3^-)$	9.2	0.03	0.11	0.02	0.10
	Sum	0.05%	0.26%	0.04%	0.25%
${}^{5}_{\Lambda_s\Lambda_s}\mathrm{H}+{}^{8}\mathrm{Be}(0^+)$	8.7	0.06	0.09	0.05	0.09
${}^{5}_{\Lambda_s\Lambda_s}\mathrm{H}+{}^{8}\mathrm{Be}(2^+)$	5.8	0.05	0.13	0.05	0.13
${}^{5}_{\Lambda_s\Lambda_s}\mathrm{H}+{}^{8}\mathrm{Be}(4^+)$	-2.7				
	Sum	0.11%	0.22%	0.10%	0.22%
${}^{9}_{\Lambda_s}\mathrm{Be}(0^+)+{}^{4}_{\Lambda_s}\mathrm{H}$	10.0	0.08	0.03	0.06	0.03
${}^{9}_{\Lambda_s}\mathrm{Be}(2^+)+{}^{4}_{\Lambda_s}\mathrm{H}$	7.1	0.14	0.04	0.11	0.03
${}^{9}_{\Lambda_s}\mathrm{Be}(4^+)+{}^{4}_{\Lambda_s}\mathrm{H}$	-1.4				
	Sum	0.22%	0.07%	0.17%	0.06%
${}^{8}_{\Lambda_s}\mathrm{Li}(1^-)+{}^{5}_{\Lambda_s}\mathrm{He}$	13.6	0.12	0.02	0.10	0.02
${}^{8}_{\Lambda_s}\mathrm{Li}(3^-)+{}^{5}_{\Lambda_s}\mathrm{He}$	7.8	0.09	0.02	0.08	0.02
	Sum	0.21%	0.04%	0.18%	0.04%

TABLE IV. *(Continued).*

		$V_{0\Xi}=16$ MeV		$V_{0\Xi}=24$ MeV	
Channel	Q (MeV)	$(2p)_\Xi$ (%)	$(3d)_\Xi$ (%)	$(2p)_\Xi$ (%)	$(3d)_\Xi$ (%)
${}^{12}_{\Lambda_s}\mathrm{B}(1^-)+\Lambda$	23.9	0.64	0.25	0.88	0.33
${}^{12}_{\Lambda_p}\mathrm{B}(2^+)+\Lambda$	12.9	0.97	0.67	1.17	0.74
${}^{12}_{\Lambda_p}\mathrm{B}(1^+)+\Lambda$	12.9	0.00	0.00	0.00	0.00
${}^{12}_{\Lambda_p}\mathrm{B}(0^+_1)+\Lambda$	12.9	0.23	0.16	0.45	0.24
${}^{12}_{\Lambda_s}\mathrm{B}(0^+_2)+\Lambda$ [a]	3.0	0.22	0.06	0.32	0.08
	Sum	2.07%	1.13%	2.82%	1.38%

[a] ${}^{12}_{\Lambda_s}\mathrm{B}(0^+_2)$ has the [^{11}B (s-hole$\otimes S_\Lambda$] configuration.

nuclear wave function with no channel coupling in the calculation of the double-Λ hypernuclear production rate for the Ξ^--atomic capture reaction. The calculated energy spectra of ${}^{12}_{\Lambda\Lambda}$B and ${}^{12}_{\Lambda\Lambda}$Be are shown in Fig. 2, in which the energy levels are assigned by the total orbital angular momentum and are degenerate in energy with respect to the nuclear core spin.

C. Intracluster potential and continuum wave function in the final channel

The intracluster potential between ${}^{A_1+2}_{\Lambda\Lambda}Z_1$ and ${}^{A_2}Z_2$ (${}^{A_1+1}_{\Lambda}Z_1$ and ${}^{A_2+1}_{\Lambda}Z_2$, ${}^{A'+1}_{\Lambda}Z'$ and Λ) is derived with the folding potential model. As the wave functions for the double-Λ hypernuclei (${}^{A+2}_{\Lambda\Lambda}Z$), single-Λ hypernuclei (${}^{A+1}_{\Lambda}Z$) and normal nuclei (${}^{A}Z$), we use those presented in the previous subsections. In this section, the isospin is ignored for simplicity.

The folding potential between ${}^{A_1+2}_{\Lambda\Lambda}Z_1$ (nuclear core part $C_1\equiv{}^{A_1}Z_1$) and ${}^{A_2}Z_2$ ($C_2\equiv{}^{A_2}Z_2$) with the total angular momentum J and the relative orbital angular momentum L referring to the relative coordinate $\mathbf{R}$ between the two clusters is given as

$$V^{\mathrm{double}-\Lambda}_{J_H LJ}(\mathbf{R})=\langle (J_{\Lambda\Lambda}I_c)J_H L;J|\sum_{i\in C_1}\sum_{j\in C_2}\{v_{NN}(i,j)+v_{\mathrm{Coulomb}}(i,j)\}+\sum_{i=1}^{2}\sum_{j\in C_2}v_{\Lambda N}(\Lambda_i,j)|(J_{\Lambda\Lambda}I_c)J_H L;J\rangle, \tag{35}$$

$$|(J_{\Lambda\Lambda}I_c)J_H L;J\rangle=[[\phi_{J_{\Lambda\Lambda}}({}^{A_1+2}_{\Lambda_1\Lambda_2}Z_1)\Phi_{I_c}({}^{A_2}Z_2)]_{J_H}Y_L(\hat{R})]_J, \tag{36}$$

where v_{Coulomb} and $v_{\Lambda N}$ denote, respectively, Coulomb and Λ-N interactions. For the Λ-N interaction, we use the one-range Gaussian-type interaction given in Eq. (29), where the strength $v^0_{\Lambda N}$ in Eq. (29) is determined so as to reproduce the experimental Λ binding energy of the ${}^{A_2}Z_2+\Lambda$ system. As

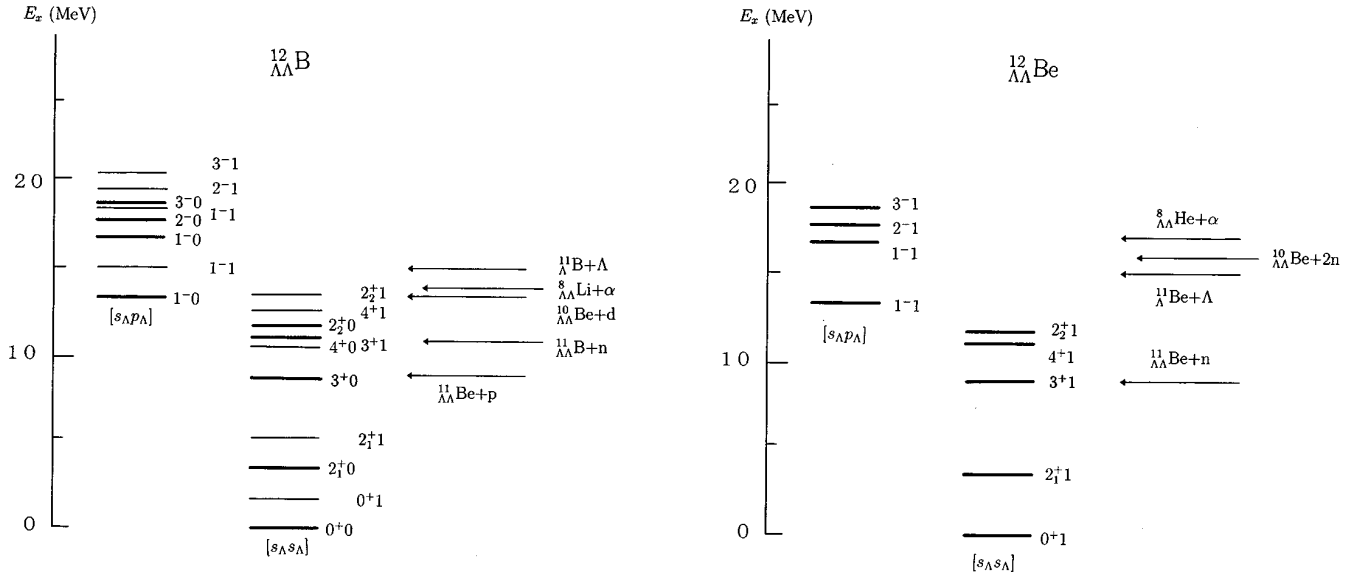

FIG. 2. Calculated energy spectra of ${}^{12}_{\Lambda\Lambda}$B and ${}^{12}_{\Lambda\Lambda}$Be, where each energy level is assigned by the total orbital angular momentum (L^π) and isospin (t). Energy levels with isospin $t=0$ for ${}^{12}_{\Lambda\Lambda}$B are degenerate in energy with respect to the nuclear-core spin ($s=1$).

for the N-N interaction denoted by v_{NN}, we employ the Hasegawa-Nagata-Yamamoto (HNY) effective interaction [16].

Concerning the twin-Λ hypernuclear channel, the folding potential between ${}^{A_1+1}_{\Lambda}Z_1$ ($C_1 \equiv {}^{A_1}Z_1$) and ${}^{A_2+1}_{\Lambda}Z_2$ ($C_2 \equiv {}^{A_2}Z_2$) with the total angular momentum J and the relative orbital angular momentum L referring to the relative coordinate $\mathbf{R}$ between the two clusters is given as

$$V^{\text{twin}-\Lambda}_{J_H L J}(\mathbf{R}) = \langle (J_{\Lambda_1} J_{\Lambda_2}) J_H L; J | \sum_{i\in C_1}\sum_{j\in C_2} \{ v_{NN}(i,j) + v_{\text{Coulomb}}(i,j)\} + \sum_{i\in C_1} v_{\Lambda N}(\Lambda_2, i) + \sum_{j\in C_2} v_{\Lambda N}(\Lambda_1, j) + v_{\Lambda\Lambda}(\Lambda_1,\Lambda_2) | (J_{\Lambda_1} J_{\Lambda_2}) J_H L; J\rangle, \quad (37)$$

$$|(J_{\Lambda_1} J_{\Lambda_2}) J_H L; J\rangle = [[\Phi_{J_{\Lambda_1}}({}^{A_1+1}_{\Lambda_1}Z_1)\Phi_{J_{\Lambda_2}}({}^{A_2+1}_{\Lambda_2}Z_2)]_{J_H} Y_L(\hat{R})]_J, \quad (38)$$

with the HNY N-N interaction (v_{NN}) and the YNG-D Λ-Λ interaction ($v_{\Lambda\Lambda}$) given in Eq. (34). As for the Λ-N interaction $v_{\Lambda N}(\Lambda_2, i)$ with $i \in C_1$ [$v_{\Lambda N}(\Lambda_1, j)$ with $j \in C_2$], we use the one-range Gaussian interaction given in Eq. (29), whose strength is chosen to reproduce the experimental Λ binding energy of the ${}^{A_1}Z_1 + \Lambda$ (${}^{A_2}Z_2 + \Lambda$) system. It should be noted that all the N-N, Λ-N, and Λ-Λ interactions are incorporated in the twin-Λ hypernuclear channel. On the other hand, the folding potential between ${}^{A'+1}_{\Lambda}Z'$ (nuclear core part $C' \equiv {}^{A'}Z'$) and Λ is given as

$$V^{\text{single}-\Lambda}_{J_H L J_\Lambda J}(\mathbf{R}) = \langle J_H L J_\Lambda; J | \sum_{i\in C'} v_{\Lambda N}(\Lambda_2, i) + v_{\Lambda\Lambda}(\Lambda_1,\Lambda_2) | J_H L J_\Lambda; J\rangle, \quad (39)$$

$$|J_H L J_\Lambda; J\rangle = [\Phi_{J_H}({}^{A'+1}_{\Lambda_1}Z')[Y_L(\hat{R})\chi_{1/2}(\Lambda_2)]_{J_\Lambda}]_J, \quad (40)$$

with $J_\Lambda = L \pm 1/2$ and the YNG-D Λ-Λ interaction ($v_{\Lambda\Lambda}$). As for the Λ-N interaction, we use the one-range Gaussian interaction given in Eq. (29), whose strength is determined to reproduce the experimental Λ binding energy of the ${}^{A'}Z' + \Lambda$ system.

The continuum wave function $\varphi_L(R, k_f)$ given in Eq. (15) is derived from solving the potential problem, in which we use the intracluster potentials given in Eqs. (35), (37), and (39). Here, we require the radial wave function $\varphi_L(R, k_f)$ to be orthogonal to the Pauli-forbidden states between the two clusters in the final channel. The Pauli-forbidden states are usually expressed as harmonic oscillator wave functions $u_{NL}(R)$. This procedure corresponds to taking into account approximately the antisymmetrization effect between the two clusters in the final channel. For example, in the ${}^{12}_{\Lambda\Lambda}\text{B}+n$, ${}^{11}_{\Lambda\Lambda}\text{Be}+d$, ${}^{9}_{\Lambda}\text{Be}+{}^{4}_{\Lambda}\text{H}$, and ${}^{8}_{\Lambda}\text{Li}+{}^{5}_{\Lambda}\text{He}$ cases, their radial wave functions must be orthogonal to the harmonic oscillator wave functions $u_{NL}(R)$ with quanta $Q = 2N + L$ less than one, two, three, and four quanta, respectively. We obtain such a continuum-state radial wave function with the use of the microscopic cluster model technique.

TABLE V. Summary of production rates per Ξ^- (R/Ξ^-) for double-Λ and single-Λ hypernuclei. See Table IV and the text.

	$V_{0\Xi} = 16$ MeV		$V_{0\Xi} = 24$ MeV	
Channel	$(2p)_\Xi$ (%)	$(3d)_\Xi$ (%)	$(2p)_\Xi$ (%)	$(3d)_\Xi$ (%)
${}^{12}_{\Lambda\Lambda}\text{B}+n$	3.96	1.47	3.35	1.45
${}^{12}_{\Lambda\Lambda}\text{Be}+p$	2.43	1.00	2.07	0.99
${}^{11}_{\Lambda\Lambda}\text{Be}+d$	0.59	2.05	0.50	2.01
${}^{10}_{\Lambda\Lambda}\text{Be}+t$	0.14	0.02	0.12	0.02
${}^{9}_{\Lambda\Lambda}\text{Li}+\alpha$	0.05	0.02	0.05	0.02
${}^{6}_{\Lambda\Lambda}\text{He}+{}^{7}\text{Li}$	0.05	0.26	0.10	0.26
${}^{5}_{\Lambda\Lambda}\text{H}+{}^{8}\text{Be}$	0.11	0.22	0.10	0.22
${}^{9}_{\Lambda}\text{Be}+{}^{4}_{\Lambda}\text{H}$	0.22	0.07	0.17	0.06
${}^{8}_{\Lambda}\text{Li}+{}^{5}_{\Lambda}\text{He}$	0.21	0.04	0.18	0.04
${}^{12}_{\Lambda}\text{B}+\Lambda$	2.07	1.13	2.82	1.38

IV. RESULTS AND DISCUSSION

The calculated production rates per Ξ^- (R/Ξ^-) for the ${}^{12}_{\Lambda\Lambda}\text{B}+n$, ${}^{12}_{\Lambda\Lambda}\text{Be}+p$, ${}^{11}_{\Lambda\Lambda}\text{Be}+d$, ${}^{10}_{\Lambda\Lambda}\text{Be}+t$, ${}^{9}_{\Lambda\Lambda}\text{Li}+\alpha$, ${}^{6}_{\Lambda\Lambda}\text{He}+{}^{7}\text{Li}$, ${}^{5}_{\Lambda\Lambda}\text{H}+{}^{8}\text{Be}$, ${}^{9}_{\Lambda}\text{Be}+{}^{4}_{\Lambda}\text{H}$, ${}^{8}_{\Lambda}\text{Li}+{}^{5}_{\Lambda}\text{He}$, and ${}^{12}_{\Lambda}\text{B}+\Lambda$ channels (including their excited channels) via the ${}^{12}\text{C}+\Xi^-$-atomic capture reaction are given in Table IV (are summarized in Table V) together with their excited channels, where the Ξ^- particle is absorbed from the $(2p)_\Xi$ and $(3d)_\Xi$ atomic orbits with the Ξ-nucleus potential strength $V_{0\Xi} = 16$ and 24 MeV. In Table IV, the notation of $\Lambda_s\Lambda_s$ ($\Lambda_s\Lambda_p$) represents the two Λ particle configuration with one Λ in the s_Λ state (s_Λ) and another in the s_Λ state (p_Λ). The KEK-E176 experimental results [2,3] for the twin-Λ hypernuclear productions and the cascade-calculation results [11] suggest the Ξ^- particles are absorbed from the $(2p)_\Xi$- or $(3d)_\Xi$-atomic orbits. On the other hand, the value of $V_{0\Xi} = 24$ MeV is derived from the old emulsion data [1]. However, the recent KEK-E224 experimental result [17] indicates that $V_{0\Xi} = 16$ MeV is preferable to reproduce the excitation function of the (K^-, K^+) reaction.

First, the dependence of the Λ-hypernuclear production rates on the $(2p)_\Xi$ and $(3d)_\Xi$ atomic states are discussed in subsections A and B, respectively. Then, we compare our calculated results with the experimental ones in the subsection C.

A. Λ-hypernuclear production via the $(2p)_\Xi$-atomic state

In the case of the $(2p)_\Xi$-atomic capture with $V_{0\Xi} = 16$ MeV, the channel with the largest production rate per Ξ^- is the ${}^{12}_{\Lambda\Lambda}\text{B}+n$ channel with $R/\Xi^- = 3.96\%$ (see Tables IV and V). The main component comes from the excited channels, ${}^{12}_{\Lambda\Lambda}\text{B}^{t=0s=1}(L^\pi = 2^+_2)+n$ ($R/\Xi^- = 2.28\%$) and ${}^{12}_{\Lambda\Lambda}\text{B}^{t=1s=0}(L^\pi = 2^+_2)+n$ ($R/\Xi^- = 0.95\%$) with the double-Λ hypernuclear configurations $[{}^{10}\text{B}^{t=0s=1}(l^\pi = 2^+_2)\otimes s_\Lambda \otimes s_\Lambda]_{L^\pi = 2^+_2}$ and $[{}^{10}\text{B}^{t=1s=0}(l^\pi = 2^+_2)\otimes s_\Lambda \otimes s_\Lambda]_{L^\pi = 2^+_2}$, re-

spectively. Here, l, s, and t denote the orbital angular momentum, spin and isospin for the nuclear core part, respectively, and L represents the total orbital angular momentum of the double-Λ hypernucleus. The second largest production-rate-per-Ξ channel is the ${}^{12}_{\Lambda\Lambda}\mathrm{Be}+p$ channel with $R/\Xi=2.43\%$, in which the main channel is the excited one ${}^{12}_{\Lambda\Lambda}\mathrm{Be}(L^{\pi}=2^{+}_{2})+p$ ($R/\Xi=2.03\%$) with the double-Λ hypernuclear configuration $[{}^{10}\mathrm{Be}^{t=1s=0}(l^{\pi}=2^{+}_{2})\otimes s_{\Lambda}\otimes s_{\Lambda}]_{L^{\pi}=2^{+}_{2}}$. The third largest one is the ${}^{11}_{\Lambda\Lambda}\mathrm{Be}+d$ channel with $R/\Xi=0.59\%$, where the main component comes from the excited channel ${}^{11}_{\Lambda\Lambda}\mathrm{Be}(L^{\pi}=3^{-})+d$ ($R/\Xi=0.42\%$) with the double-Λ hypernuclear configuration $[{}^{9}\mathrm{Be}^{t=1/2\ s=1/2}(l^{\pi}=3^{-})\otimes s_{\Lambda}\otimes s_{\Lambda}]_{L^{\pi}=3^{-}}$.

From Table IV, we notice that the production rates per Ξ of the excited channels, ${}^{12}_{\Lambda\Lambda}\mathrm{B}(L^{\pi}=2^{+}_{2})+n$ and ${}^{12}_{\Lambda\Lambda}\mathrm{Be}(L^{\pi}=2^{+}_{2})+p$, are larger than those of their ground-state channels, ${}^{12}_{\Lambda\Lambda}\mathrm{B}(L^{\pi}=0^{+})+n$ and ${}^{12}_{\Lambda\Lambda}\mathrm{Be}(L^{\pi}=0^{+})+p$. There are two reasons why the excited channels of ${}^{12}_{\Lambda\Lambda}\mathrm{B}+n$ and ${}^{12}_{\Lambda\Lambda}\mathrm{Be}+p$ have the larger production rates than the ground-state channels. As an example, in the case of the ${}^{12}_{\Lambda\Lambda}\mathrm{B}+n$ channel, we discuss them as follows: In the direct reaction picture, the Ξ^{-} particle in an atomic state interacts with a proton in ${}^{12}\mathrm{C}$ to produce the highly excited double-Λ hypernculear state with the configuration of $[{}^{11}\mathrm{B}(\text{proton-hole})\otimes\Lambda\otimes\Lambda]$ as an intermediate state, and then it is fragmented mainly at the doorway stage to the channels ${}^{A_1}_{\Lambda\Lambda}Z_1+{}^{A_2}Z_2$, ${}^{A_1}_{\Lambda}Z_1+{}^{A_2}_{\Lambda}Z_2$, etc. according to the fragmentation mode of the nuclear-core proton-hole state:

$$
\begin{aligned}
({}^{12}C,\Xi^{-})_{\text{atom}} &\rightarrow [{}^{11}\mathrm{B}(\text{proton-hole})\oplus\Lambda\oplus\Lambda] \\
&\rightarrow [({}^{A_1}Z_1+{}^{A_2}Z_2)\oplus\Lambda\oplus\Lambda] \\
&\rightarrow {}^{A_1+2}_{\Lambda\Lambda}Z_1+{}^{A_2}Z_2,\ {}^{A_1+1}_{\Lambda}Z_1+{}^{A_2+1}_{\Lambda}Z_2,\quad \text{etc.}
\end{aligned}
\tag{41}
$$

Therefore, increasing the value of the spectroscopic factor for the fragmentation of ${}^{11}\mathrm{B}$ to two-body channels $({}^{A_1}Z_1+{}^{A_2}Z_2)$ leads to a larger production rate of double-Λ hypernuclei $({}^{A_1+2}_{\Lambda\Lambda}Z_1+{}^{A_2}Z_2$ or ${}^{A_2+2}_{\Lambda\Lambda}Z_2+{}^{A_1}Z_1)$. Table VI shows the spectroscopic factors S^2 for the fragmentation of ${}^{11}\mathrm{B}$ to two-body channels $({}^{A_1}Z_1+{}^{A_2}Z_2)$. We see that the spectroscopic factor for ${}^{11}\mathrm{B}(p\text{-hole})\rightarrow{}^{10}\mathrm{B}^{t=0s=1}(2^{+}_{2})+n$ $[{}^{10}\mathrm{B}^{t=0s=1}(0^{+})+n]$ is as large as $S^2=2.36$ (1.10). It is noted that this characteristic persists also in the case of using the Cohen-Kurath wave functions [18], although their components are dispersed in some states of ${}^{11}\mathrm{B}$ due to the spin coupling of $\mathbf{j}=\mathbf{l}+\mathbf{s}$. This is one of the important reasons why the excited channels of ${}^{12}_{\Lambda\Lambda}\mathrm{B}+n$ and ${}^{12}_{\Lambda\Lambda}\mathrm{Be}+p$ have the production rate larger than that for the ground-state channels. The other important reason is given as follows: Reflecting the fact that the Q value for ${}^{12}_{\Lambda\Lambda}\mathrm{B}^{t=0s=1}(L^{\pi}=2^{+}_{2})+n$ ($Q=14.1$ MeV) is smaller than that for ${}^{12}_{\Lambda\Lambda}\mathrm{B}^{t=0s=1}(L^{\pi}=0^{+})+n$ ($Q=26.0$ MeV), the former channel has a broad resonancelike state with the relative orbital angular momentum $L^{\pi}_{R}=3^{-}$ between ${}^{12}_{\Lambda\Lambda}\mathrm{B}$ and n around the ${}^{12}\mathrm{C}+\Xi^{-}$ threshold, while the latter channel does not have such a resonant state. It is noted that the total angular momentum (J^{π}) of the ${}^{12}_{\Lambda\Lambda}\mathrm{B}+n$ system is $J^{\pi}=1^{-}$, and the height of the centrifugal barrier for the $L^{\pi}_{R}=3^{-}$ partial wave is as large as about 12 MeV, which is estimated from the ${}^{12}_{\Lambda\Lambda}\mathrm{B}-n$ folding potential plus the centrifugal potential. Even if taking into account the spin-orbit splitting between ${}^{12}_{\Lambda\Lambda}\mathrm{B}$ and n, the broad resonancelike state with $L^{\pi}_{R}=3^{-}$ might persist around ${}^{12}\mathrm{C}+\Xi^{-}$ threshold due to the broad width (~ 5 MeV). (For the $L^{\pi}_{R}=1^{-}$ partial wave of the ${}^{12}_{\Lambda\Lambda}\mathrm{B}^{t=0s=1}(L^{\pi}=2^{+}_{2})+n$ channel, the height of the centrifugal barrier is about a few MeV, so that its contribution to the production of the ${}^{12}_{\Lambda\Lambda}\mathrm{B}^{t=0s=1}(L^{\pi}=2^{+}_{2})+n$ channel becomes small in comparion with the case for the $L^{\pi}_{R}=3^{-}$.) The above-mentioned two reasons lead to the considerably larger value of ρ^{DW}_{fi} [see Eq. (7)] for the ${}^{12}_{\Lambda\Lambda}\mathrm{B}^{t=0s=1}(2^{+}_{2})+n$ channel than that for the ${}^{12}_{\Lambda\Lambda}\mathrm{B}^{t=0s=1}(0^{+})+n$ channel, although the value of the phase space $k_f\omega_f$ for the former is somewhat smaller than that for the latter [see Eq. (9)]. Therefore, the production rate per Ξ for the ${}^{12}_{\Lambda\Lambda}\mathrm{B}^{t=0s=1}(2^{+}_{2})+n$ channel becomes larger than that for the ${}^{12}_{\Lambda\Lambda}\mathrm{B}^{t=0s=1}(0^{+})+n$ channel.

From Fig. 2, we note that the ${}^{12}_{\Lambda\Lambda}\mathrm{B}^{t=0s=1}(L^{\pi}=2^{+}_{2})$ state can be fragmented to the ${}^{11}_{\Lambda\Lambda}\mathrm{B}+n$ and ${}^{11}_{\Lambda\Lambda}\mathrm{Be}+p$ channels as well as the γ decay. Then, the following process is possible:

$$
\begin{aligned}
({}^{12}\mathrm{C},\Xi^{-})_{2p\text{-atom}} &\rightarrow {}^{12}_{\Lambda\Lambda}\mathrm{B}^{*}+n \\
&\rightarrow {}^{11}_{\Lambda\Lambda}\mathrm{Be}+p+n,\ {}^{11}_{\Lambda\Lambda}\mathrm{B}+n+n,\quad \text{etc.}
\end{aligned}
\tag{42}
$$

TABLE VI. Calculated spectroscopic factors (S^2) for the fragmentation of ${}^{11}\mathrm{B}$ to two-body channels $({}^{A_1}Z_1+{}^{A_2}Z_2)$, where l^{π} denotes the relative orbital angular momentum between ${}^{A_1}Z_1$ and ${}^{A_2}Z_2$. The $\mathrm{SU}(3)(\lambda\mu)_{L^{\pi}}=(13)_{1^{-}}$ and $(04)_{0^{+}}$ states correspond to the p-hole and s-hole states of ${}^{11}\mathrm{B}$.

	${}^{11}\mathrm{B}(\lambda\mu)_{L^{\pi}}=(13)_{1^{-}}$		${}^{11}\mathrm{B}(\lambda\mu)_{L^{\pi}}=(04)_{0^{+}}$	
Channel	l^{π}	S^2	l^{π}	S^2
${}^{10}\mathrm{B}^{T=0}(0^{+})+n$	1^{-}	1.10	0^{+}	0.03
${}^{10}\mathrm{B}^{T=0}(2^{+}_{1})+n$	1^{-}	0.25	2^{+}	0.01
${}^{10}\mathrm{B}^{T=0}(2^{+}_{2})+n$	1^{-}	2.36	2^{+}	0.07
${}^{10}\mathrm{B}^{T=1}(0^{+})+n$	1^{-}	0.37	0^{+}	0.01
${}^{10}\mathrm{B}^{T=1}(2^{+}_{1})+n$	1^{-}	0.08	2^{+}	0.00
${}^{10}\mathrm{B}^{T=1}(2^{+}_{2})+n$	1^{-}	0.79	2^{+}	0.02
${}^{10}\mathrm{Be}(0^{+})+p$	1^{-}	0.73	0^{+}	0.02
${}^{10}\mathrm{Be}(2^{+}_{1})+p$	1^{-}	0.17	2^{+}	0.00
${}^{10}\mathrm{Be}(2^{+}_{2})+p$	1^{-}	1.58	2^{+}	0.05
${}^{9}\mathrm{Be}(1^{-})+d$	0^{+}	1.00	1^{-}	0.18
	2^{+}	0.80		
${}^{9}\mathrm{Be}(3^{-})+d$	2^{+}	1.60	3^{-}	0.16
${}^{8}\mathrm{Be}(0^{+})+t$	1^{-}	0.41	0^{+}	0.14
${}^{8}\mathrm{Be}(2^{+})+t$	1^{-}	0.36	2^{+}	0.17
	3^{-}	0.15		
${}^{8}\mathrm{Be}(4^{+})+t$	3^{-}	0.52	4^{+}	0.17
${}^{7}\mathrm{Li}(1^{-})+\alpha$	0^{+}	0.41	1^{-}	0.00
	2^{+}	0.36		
${}^{7}\mathrm{Li}(3^{-})+\alpha$	2^{+}	0.15	3^{-}	0.00
	4^{+}	0.51		

The sequential process is the same as the production process of ${}^{13}_{\Lambda\Lambda}$B observed in the KEK-E176 experiment [2,3], $({}^{14}\mathrm{N},\Xi^-)_{\mathrm{atom}} \rightarrow {}^{14}_{\Lambda\Lambda}\mathrm{C}^* + n \rightarrow {}^{13}_{\Lambda\Lambda}\mathrm{B} + p + n$. This result supports the interpretation of Dover *et al.*, [4] for the double-Λ hypernucleus observed in the KEK-E176 experiment [2,3].

The fourth largest production-rate-per-Ξ channel is the ${}^{10}_{\Lambda\Lambda}\mathrm{Be}+t$ channel with $R_\Xi = 0.14\%$, in which the values of R/Ξ for the ${}^{10}_{\Lambda\Lambda}\mathrm{Be}(0^+)+t$, ${}^{10}_{\Lambda\Lambda}\mathrm{Be}(2^+)+t$, and ${}^{10}_{\Lambda\Lambda}\mathrm{Be}(4^+)+t$ channels are 0.06, 0.06, and 0.02%, respectively. As for the ${}^{5}_{\Lambda\Lambda}\mathrm{H}+{}^{8}\mathrm{Be}$, ${}^{9}_{\Lambda\Lambda}\mathrm{Li}+\alpha$, and ${}^{6}_{\Lambda\Lambda}\mathrm{He}+{}^{7}\mathrm{Li}$ channels, their production rates per Ξ are $R/\Xi = 0.11$, 0.05, and 0.05%. The reason why the production rates for ${}^{10}_{\Lambda\Lambda}\mathrm{Be}+t$, ${}^{9}_{\Lambda\Lambda}\mathrm{Li}+\alpha$, ${}^{6}_{\Lambda\Lambda}\mathrm{He}+{}^{7}\mathrm{Li}$, and ${}^{5}_{\Lambda\Lambda}\mathrm{H}+{}^{8}\mathrm{Be}$ are smaller than those for ${}^{12}_{\Lambda\Lambda}\mathrm{B}+n$, ${}^{12}_{\Lambda\Lambda}\mathrm{Be}+p$ and ${}^{11}_{\Lambda\Lambda}\mathrm{Be}+d$ is due to the following facts: (1) the spectroscopic factors for the fragmentation of ^{11}B to the ${}^{10}\mathrm{B}+n$, ${}^{10}\mathrm{Be}+p$ and ${}^{9}\mathrm{Be}+d$ channels are considerably larger than those to the ${}^{8}\mathrm{Be}+t$ and ${}^{7}\mathrm{Li}+\alpha$ channels (see Table VI), and (2) the Q values for ${}^{12}_{\Lambda\Lambda}\mathrm{B}+n$, ${}^{12}_{\Lambda\Lambda}\mathrm{Be}+p$, and ${}^{11}_{\Lambda\Lambda}\mathrm{Be}+d$ are larger than those for ${}^{10}_{\Lambda\Lambda}\mathrm{Be}+t$, ${}^{9}_{\Lambda\Lambda}\mathrm{Li}+\alpha$, ${}^{6}_{\Lambda\Lambda}\mathrm{He}+{}^{7}\mathrm{Li}$, and ${}^{5}_{\Lambda\Lambda}\mathrm{H}+{}^{8}\mathrm{Be}$, and therefore, the values of the phase space for the former channels become large in comparison with those for the latter. It is noted that the compound double-Λ hypernuclear picture [9] predicts the very large production rate of ${}^{6}_{\Lambda\Lambda}$He. However, the KEK-E176 experimental data showed no evidence of ${}^{6}_{\Lambda\Lambda}$He [2,3]. Our calculated result that the production rate per Ξ for the ${}^{6}_{\Lambda\Lambda}\mathrm{He}+{}^{7}\mathrm{Li}$ channel is as small as 0.05% is consistent with the experimental data.

Concerning the twin-Λ hypernuclear production, the R/Ξ for the ${}^{9}_{\Lambda}\mathrm{Be}+{}^{4}_{\Lambda}\mathrm{H}$ channel is 0.22% with $R/\Xi[{}^{9}_{\Lambda}\mathrm{Be}+(0^+)+{}^{4}_{\Lambda}H] = 0.08\%$ and $R/\Xi[{}^{9}_{\Lambda}\mathrm{Be}+(2^+)+{}^{4}_{\Lambda}\mathrm{H}] = 0.14\%$. It is noted that the ${}^{9}_{\Lambda}\mathrm{Be}(4^+)+{}^{4}_{\Lambda}\mathrm{H}$ channel is forbidden because of its negative Q value (see Fig. 1). On the other hand, the R/Ξ for the ${}^{8}_{\Lambda}\mathrm{Li}+{}^{5}_{\Lambda}\mathrm{He}$ channel is 0.21% with $R/\Xi[{}^{8}_{\Lambda}\mathrm{Li}(1^-)+{}^{5}_{\Lambda}\mathrm{He}] = 0.12\%$ and $R/\Xi[{}^{8}_{\Lambda}\mathrm{Li}+(3^-)+{}^{5}_{\Lambda}\mathrm{He}] = 0.09\%$. In both the twin-$\Lambda$ hypernuclear channels, the R/Ξ value for the excited channel is almost the same as or larger than that for the ground-state channel. This is the characteristic of our model, as will be shown also in the $(3d)_\Xi$-atomic capture case (see Sec. IV B). The reason, for example, in the ${}^{9}_{\Lambda}\mathrm{Be}+{}^{4}_{\Lambda}\mathrm{H}$ channel, is given as follows: (1) the spectroscopic factors for the ${}^{11}\mathrm{B}(p\text{-hole}) \rightarrow {}^{8}\mathrm{Be}(2^+)+t$ channel is almost the same as those for ${}^{11}\mathrm{B} \rightarrow {}^{8}\mathrm{Be}(0^+)+t$ (see Table VI), and (2) the difference of the Q value between the ${}^{9}_{\Lambda}\mathrm{Be}(0^+)+{}^{4}_{\Lambda}\mathrm{H}$ and ${}^{9}_{\Lambda}\mathrm{Be}(2^+)+{}^{4}_{\Lambda}\mathrm{H}$ channels is not so large ($\sim$3 MeV). The same situation is realized also in the ${}^{8}_{\Lambda}\mathrm{Li}+{}^{5}_{\Lambda}\mathrm{He}$ channel. When we compare the values of the production rates per Ξ for the twin-Λ hypernuclear production channels with those for the ${}^{12}_{\Lambda\Lambda}\mathrm{B}+n$ and ${}^{12}_{\Lambda\Lambda}\mathrm{Be}+p$ channels, the production rates per Ξ for the double-Λ hypernuclei are larger than those for the twin-Λ hypernuclei. This is due to the fact that (1) the spectroscopic factors for ${}^{11}\mathrm{B} \rightarrow {}^{8}\mathrm{Be}+t$ and ${}^{7}\mathrm{Li}+\alpha$ are smaller than those for ${}^{11}\mathrm{B} \rightarrow {}^{10}\mathrm{B}+n$ and ${}^{10}\mathrm{Be}+p$ (see Table VI), and (2) the ${}^{12}_{\Lambda\Lambda}\mathrm{B}+n$ and ${}^{12}_{\Lambda\Lambda}\mathrm{Be}+p$ channels have broad resonancelike states around the ${}^{12}\mathrm{C}+\Xi^-$ threshold, while the twin-Λ channels do not have such states in the present calculation.

As for the ${}^{12}_{\Lambda}\mathrm{B}+\Lambda$ channel, the total production rate per Ξ is $R/\Xi = 2.07\%$. We see that the R/Ξ for the excited channel ${}^{12}_{\Lambda}\mathrm{B}(L^\pi = 2^+)+\Lambda$ with the single-Λ hypernuclear configuration $[{}^{11}\mathrm{B}(1^-)\otimes p_\Lambda]_{L^\pi=2^+}$ is largest and amounts to 0.97%, and the secondary largest channel is the ground-state channel ${}^{12}_{\Lambda}\mathrm{B}(L^\pi = 1^-)+\Lambda$ ($R/\Xi = 0.64\%$) with the single-Λ hypernuclear configuration $[{}^{11}\mathrm{B}(1^-)\otimes s_\Lambda]_{L^\pi=1^-}$. It is noted that the excited hypernuclear state ${}^{12}_{\Lambda}\mathrm{B}(L^\pi = 2^+)$ is produced as much as the ground state of ${}^{12}_{\Lambda}$B in our calculation.

TABLE VII. Calculated Ξ binding energies for the $\Xi^- + {}^{12}$C hypernuclear and atomic states with the Woods-Saxon potential strength $V_{0\Xi} = 16$ and 24 MeV [see Eq. (12)]. In the table, H.N. and atom denote, respectively, the Ξ hypernuclear and atomic states.

	$V_{0\Xi} = 24$ MeV		$V_{0\Xi} = 16$ MeV	
	B_Ξ (MeV)		B_Ξ (MeV)	
$(1s)_\Xi$	11.51	H.N.	6.71	H.N.
$(1p)_\Xi$	2.25	H.N.		
$(2s)_\Xi$	0.55	Atom	0.46	Atom
$(2p)_\Xi$	0.24	Atom	0.55	Atom
$(3d)_\Xi$	0.13	Atom	0.13	Atom

The calculated production rates per Ξ for the $(2p)_\Xi$-atomic capture in the case of $V_{0\Xi} = 24$ MeV are listed in Tables IV and V together with those in the case of $V_{0\Xi} = 16$ MeV. As shown in Table VII, the Ξ binding energy B_Ξ for the $(2p)_\Xi$-atomic state with $V_{0\Xi} = 16$ MeV ($B_\Xi = 0.55$ MeV) is larger than that with $V_{0\Xi} = 24$ MeV ($B_\Xi = 0.24$ MeV). This reason is given as follows: In the case of $V_{0\Xi} = 24$ MeV, there appear two Ξ hypernuclear bound states, namely, the ground state (Ξ particle in the s state) with $B_\Xi = 11.51$ MeV [denoted as $(1s)_\Xi$] and excited state (Ξ particle in the p state) with $B_\Xi = 2.25$ MeV [denoted as $(1p)_\Xi$], together with the Ξ-atomic states, $(2s)_\Xi$, $(2p)_\Xi$, $(3d)_\Xi$, etc. (see Table VII). On the other hand, in the case of $V_{0\Xi} = 16$ MeV, there appears only one Ξ hypernuclear bound state, namely, the ground hypernuclear state with $B_\Xi = 6.71$ MeV [denoted as $(1s)_\Xi$], together with the Ξ-atomic states, $(2s)_\Xi$, $(2p)_\Xi$, $(3d)_\Xi$, etc. [see Table VII]. Since the $(1p)_\Xi$-hypernuclear state does not appear in the case of $V_{0\Xi} = 16$ MeV, the $(2p)_\Xi$-atomic state for $V_{0\Xi} = 16$ MeV corresponds to the $(1p)_\Xi$-hypernuclear state for $V_{0\Xi} = 24$ MeV. Therefore, the Ξ binding energy of the $(2p)_\Xi$-atomic state for $V_{0\Xi} = 24$ MeV which has one node in the radial wave function (the nodal point is outside the radius of ^{12}C) is smaller than that for $V_{0\Xi} = 16$ MeV which has no node in the radial wave function. This binding energy difference leads to somewhat smaller values for the calculated results of the production rates per Ξ for $V_{0\Xi} = 24$ MeV than those for $V_{0\Xi} = 16$ MeV. However, the qualitative difference between them is not clearly seen in Tables IV and V.

It is an interesting problem in the Λ-hypernuclear production reaction via the Ξ^--atomic capture whether the Ξ^- particle in an atomic orbit interacts mainly with a proton in the s or p states in ^{12}C. Since the Q value for the elementary process $\Xi^- + p \rightarrow \Lambda + \Lambda$ is 28 MeV, which is almost the same as the separation energy of an s-state proton in ^{12}C or light nuclei, the fragmentation mode of the ${}^{11}\mathrm{B}(s\text{-hole})$ state might play a more important role than that of the p-hole state

of ^{11}B. However, in the present calculation, the Ξ^- particle interacts mainly a p-state proton in ^{12}C, when it is absorbed from the $(2p)_\Xi$-atomic orbit as well as $(3d)_\Xi$. The reasons are given as follows: (1) the number of p-state protons interacting with a Ξ^- particle in an atomic orbit is larger than that of the s-state ones, (2) the spectroscopic factor for the fragmentation of the ground state of ^{12}C to ^{11}B(p-hole) and a p-state proton is considerably larger than that to ^{11}B (s-hole) and an s-state proton, when we use the SU(3) wave functions [see Eq. (11)], (3) the spectroscopic factors for the fragmentation of the ^{11}B(p-hole) state to two-body clusters are generally larger than those of ^{11}B(s-hole) (see Table VI), (4) the $^1S_0$-wave type conversion for $\Xi^- + p \to \Lambda + \Lambda$ favors that the total sum of the orbital angular momentum for the Ξ^- particle (l_Ξ) and the one for the interacting proton in ^{12}C (l_p) is zero, namely, that the selection rule of $l_p = l_\Xi$ or $l_p \simeq l_\Xi$ [8] is realized, and finally, (5) the overlap of the Ξ^--atomic wave function with the p-state proton wave function is larger than that with the s-state proton wave function. Therefore, the contribution from the ^{11}B(s-hole) state is one-order or two-orders smaller than that from ^{11}B(p-hole) in the $(2p)_\Xi$-atomic capture reaction as well as $(3d)_\Xi$. However, in the Λ-hypernuclear production reaction via the $(2s)_\Xi$-atomic state, or, in Ξ-hypernuclear states with the Ξ particle in the s-orbit, the contribution from the nuclear s-hole state is comparable to that from the nuclear p-hole state. The reason is due to the selection rule of $l_p = l_\Xi$ and, in the Ξ-hypernuclear cases, due to the goodness of the overlap of the Ξ^--particle wave function with the s-state proton wave function.

B. Λ-hypernuclear production via the $(3d)_\Xi$-atomic state

The Λ-hypernuclear production rates per Ξ (R/Ξ) in the case of the $(3d)_\Xi$-atomic state with $V_{0\Xi} = 16$ and 24 MeV are shown also in Tables IV and V. Since the $(3d)_\Xi$ state is the pure atomic state, the effect of the Ξ^--nucleus potential on the Ξ^--atomic wave function is very small. Therefore, the quantitative difference between the calculated production rates of $V_{0\Xi} = 16$ and 24 MeV are not seen at all in Tables IV and V. Hereafter, we discuss only the results of $V_{0\Xi} = 16$ MeV.

The largest production-rate-per-Ξ channel is the $^{11}_{\Lambda\Lambda}$Be$+d$ channel with $R/\Xi = 2.05\%$. The main component comes from the $^{11}_{\Lambda\Lambda}\mathrm{Be}(L^\pi = 2^+_1) + d$ channel with the configuration of $^{11}_{\Lambda\Lambda}\mathrm{Be}(L^\pi = 2^+_1) = [^9\mathrm{Be}^{t=1/2 s=1/2}(l = 1^-) \otimes s_\Lambda \otimes p_\Lambda]_{L^\pi = 2^+_1}$ ($R/\Xi = 1.68\%$). It should be noted that in $^{11}_{\Lambda_s\Lambda_p}\mathrm{Be}(L^\pi = 2^+_1)$ one Λ particle is in the s state and another in the p state. The secondary largest production-rate-per-Ξ channel is the $^{12}_{\Lambda\Lambda}$B$+n$ channel with $R/\Xi = 1.47\%$, in which the main channel is the excited channel $^{12}_{\Lambda\Lambda}\mathrm{B}^{t=0 s=1}(L^\pi = 1^-_1) + n$ with the configuration of $^{12}_{\Lambda\Lambda}\mathrm{B}^{t=0 s=1}(L^\pi = 1^-_1) = [^{10}\mathrm{B}^{t=0 s=1}(l = 0^+) \otimes s_\Lambda \otimes p_\Lambda]_{L^\pi = 1^-_1}$ ($R/\Xi = 0.91\%$). The third largest one is the $^{12}_{\Lambda\Lambda}$Be$+p$ channel with $R/\Xi = 1.00\%$, where the main component comes from the $^{12}_{\Lambda\Lambda}\mathrm{Be}^{t=1 s=0} + p$ one ($R/\Xi = 0.91\%$) with the $(s_\Lambda p_\Lambda)$ configuration.

Here, it is interesting to compare the above results with those for the $(2p)_\Xi$-atomic capture case. We find that in both the atomic cases the production rates per Ξ for the excited channels are larger than those for the ground-state channels. The reason is the same as that given in the case of the $(2p)_\Xi$-atomic capture (see Sec. IV A). On the other hand, in the $(3d)_\Xi$-atomic capture reaction, the double-Λ hypernuclei with the $(s_\Lambda p_\Lambda)$ configuration are produced more strongly than those with the (s^2_Λ) configuration in our calculation. This feature is in contrast to the case of the $(2p)_\Xi$-atomic capture, in which the two Λ particles for the largest production-rate-per-Ξ channel, $^{12}_{\Lambda\Lambda}$B$+n$, occupy mainly in the $(s_\Lambda)^2$ configuration. The reason is given as follows: As discussed in Sec. IV A, the Ξ^- particle in the atomic state $(n_\Xi l_\Xi)$ interacts mainly with a $(0p)$-state proton in ^{12}C. Owing to the $^1S_0$-wave-type conversion for $\Xi^- + p \to \Lambda + \Lambda$, the two Λ particles produced by the $(2p)_\Xi$-atomic capture reaction should occupy mainly in the $(s_\Lambda)^2$ configuration due to the parity conservation for the t matrix $\langle \Lambda\Lambda | v_{\Xi^- p \to \Lambda\Lambda}(^1S_0) | (2p)_{\Xi\text{-atom}} (0p)_{\text{proton}} \rangle$. However, in the $(3d)_\Xi$-atomic capture, the two Λ particles produced should occupy mainly in the $(s_\Lambda p_\Lambda)$ configuration due to the parity conservation for the t matrix $\langle \Lambda\Lambda | v_{\Xi^- p \to \Lambda\Lambda}(^1S_0) | (3d)_{\Xi\text{-atom}} (0p)_{\text{proton}} \rangle$. Therefore, the double-Λ hypernuclei with the $(s_\Lambda p_\Lambda)$ configuration are produced largely in the $(3d)_\Xi$-atomic capture. This is a *selection rule* for the double-Λ hypernuclei produced by the Ξ^--atomic capture reaction.

Another reason why the double-Λ hypernuclei with the $(s_\Lambda p_\Lambda)$ configuration are produced largely in the $(3d)_\Xi$-atomic capture is given as a resonant effect as follows: In the $(3d)_\Xi$-atomic capture, the orbital angular momentum $L^\pi = 2^+$ is transferred to the $^{A_1}_{\Lambda\Lambda}Z_1 + ^{A_2}Z_2$ system. In our calculation, there appear broad resonancelike states with $L^\pi = 2^+$ around the ^{12}C$+\Xi^-$ threshold for the $^{11}_{\Lambda\Lambda}$Be$+d$ and $^{12}_{\Lambda\Lambda}$B$+n$ channels with the $(s_\Lambda p_\Lambda)$ configuration, since their Q values measured from the ^{12}C$+\Xi^-$ threshold are 5–12 MeV, for which the values allow the formation of broad resonantlike states around the ^{12}C$+\Xi^-$ threshold. Therefore, their production rates become as large as $R/\Xi = 1.47$–2.05% as mentioned above. For the $^{11}_{\Lambda\Lambda}$Be$+d$ and $^{12}_{\Lambda\Lambda}$B$+n$ channels with the (s^2_Λ) configuration, there are no such resonancelike states around the ^{12}C$+\Xi^-$ threshold and therefore, their production rates are not enhanced. On the other hand, for the $(2p)_\Xi$-atomic capture, the situation is reversed. In this case, there appear broad resonancelike states with $L^\pi = 1^-$ around the ^{12}C$+\Xi^-$ threshold for the $^{12}_{\Lambda\Lambda}$B$+n$ and $^{12}_{\Lambda\Lambda}$B$+p$ channels with the (s^2_Λ) configuration, while such resonantlike states do not appear for those with the $(s_\Lambda p_\Lambda)$ configuration.

As shown in Fig. 3, the $^{11}_{\Lambda\Lambda}\mathrm{Be}(L^\pi = 2^+_1)$ state produced largely for the $(3d)_\Xi$-atomic orbit can decay to the $^{10}_{\Lambda\Lambda}$Be$+n$ and $^{10}_{\Lambda}$Be$+\Lambda$ channels as well as the γ decay. Then, the following sequential decay is possible:

$$(^{12}C, \Xi^-)_{3d\text{-atom}} \to {}^{11}_{\Lambda\Lambda}\mathrm{Be}^* + d \to {}^{10}_{\Lambda\Lambda}\mathrm{Be} + n + d$$

$$\text{and } {}^{10}_{\Lambda}\mathrm{Be} + \Lambda + d. \tag{43}$$

On the other hand, the $^{12}_{\Lambda\Lambda}\mathrm{B}^{t=0 s=1}(L^\pi = 1^-_1)$ state can decay

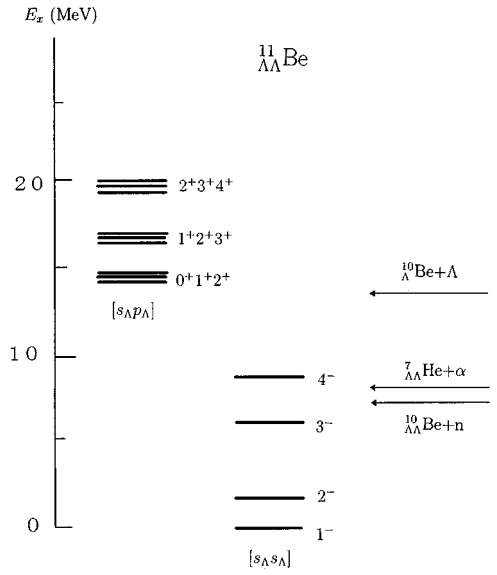

FIG. 3. Calculated energy spectra of $^{11}_{\Lambda\Lambda}$Be, where each energy level is assigned by the total orbital angular momentum (L^π), and degenerate in energy with respect to the nuclear-core spin ($s=1/2$).

to the $^{11}_{\Lambda\Lambda}$B$+n$ and $^{11}_{\Lambda\Lambda}$Be$+p$ channels as well as the γ decay as shown in Fig. 2. Therefore, the following process is possible:

$$(^{12}\mathrm{C},\Xi^-)_{3d\text{-atom}}\rightarrow {}^{12}_{\Lambda\Lambda}\mathrm{B}^*+n\rightarrow {}^{11}_{\Lambda\Lambda}\mathrm{B}+n+n$$

$$\text{and } {}^{11}_{\Lambda}\mathrm{Be}+p+n. \tag{44}$$

This process reminds us of the sequential process for the $^{13}_{\Lambda\Lambda}$B production observed in the KEK-E176 experiment, $(^{14}\mathrm{N},\Xi^-)_{\mathrm{atom}}\rightarrow {}^{14}_{\Lambda\Lambda}\mathrm{C}^*+n\rightarrow {}^{13}_{\Lambda\Lambda}\mathrm{B}+p+n$, as discussed in the $(2p)_\Xi$-atomic capture case [2,3].

Concerning the $^{10}_{\Lambda\Lambda}$Be$+t$, $^{9}_{\Lambda\Lambda}$Li$+\alpha$, $^{6}_{\Lambda\Lambda}$He$+^7$Li, and $^{5}_{\Lambda\Lambda}$H$+^8$Be channels, their production rates per Ξ are $R/\Xi=0.02$, 0.02, 0.26, and 0.22%, respectively. These values are smaller than those for $^{12}_{\Lambda\Lambda}$B$+n$, $^{12}_{\Lambda\Lambda}$Be$+p$, and $^{11}_{\Lambda\Lambda}$Be$+d$. The reasons are the Q-value effect and the magnitude of spectroscopic factors, which are the same as those given in the case of the $(2p)_\Xi$-atomic capture.

As for the twin-Λ hypernuclear channels, the ^{9}Be$+^4$H production rate per Ξ is $R/\Xi=0.07\%$ with $R/\Xi[^9_\Lambda\mathrm{Be}(0^+)+^4_\Lambda\mathrm{H}]=0.03\%$ and $R/\Xi[^9_\Lambda\mathrm{Be}(2^+)+^4_\Lambda\mathrm{H}]=0.04\%$. On the other hand, the R/Ξ for the $^8_\Lambda$Li$+^5_\Lambda$He channel is 0.04% with $R/\Xi[^8_\Lambda\mathrm{Li}(1^-)+^5_\Lambda\mathrm{He}]=0.02\%$ and $R/\Xi[^8_\Lambda\mathrm{Li}(3^-)+^5_\Lambda\mathrm{He}]=0.02\%$. In both channels, the value of R/Ξ for the excited channel is almost the same as or larger than that for the ground-state channel. This feature is the same as that in the case of the $(2p)_\Xi$ capture.

For the single-Λ hypernuclear channel, the total production rate per Ξ for $^{12}_\Lambda$B$+\Lambda$ is $R/\Xi=1.13\%$. The main component comes from the excited channel $^{12}_\Lambda\mathrm{B}(L^\pi=2^+)+\Lambda$ with the single-Λ hypernuclear configuration $[^{11}\mathrm{B}(1^-)\otimes p_\Lambda]_{L^\pi=2^+}$ ($R/\Xi=0.67\%$). The second largest channel is the ground-state one, $^{12}_\Lambda\mathrm{B}(L^\pi=1^-)+\Lambda$ ($R/\Xi=0.25\%$) with the single-Λ hypernuclear configuration $[^{11}\mathrm{B}(1^-)\otimes s_\Lambda]_{L^\pi=1^-}$. The characteristics are the same as that in the $(2p)_\Xi$-atomic capture case.

TABLE VIII. Calculated production rates per Ξ (R/Ξ) averaged over the absorption rates in the case of $V_{0\Xi}=16$ MeV.

Channel	R/Ξ (%)
$^{12}_{\Lambda\Lambda}$B$+n$	1.48
$^{12}_{\Lambda\Lambda}$Be$+p$	0.99
$^{11}_{\Lambda\Lambda}$Be$+d$	1.81
$^{10}_{\Lambda\Lambda}$Be$+t$	0.02
$^{9}_{\Lambda\Lambda}$Li$+\alpha$	0.02
$^{6}_{\Lambda\Lambda}$He$+^7$Li	0.23
$^{5}_{\Lambda\Lambda}$H$+^8$Be	0.20
$^{9}_{\Lambda}$Be$+^4_\Lambda$H	0.07
$^{8}_{\Lambda}$Li$+^5_\Lambda$He	0.04
$^{12}_{\Lambda}$B$+\Lambda$	1.08

C. Comparison with the experimental data

The calculation of the Λ-hypernuclear production rate per Ξ given in Eq. (3) assumed the transition from single orbit (n_Ξ,l_Ξ) of the Ξ^- atom. In order to compare our results with the KEK-E176 experimental results, we have to average the calculated Λ-hypernuclear production rates over the distribution $p(n_\Xi,l_\Xi)$ involved in the Ξ^- capture process. As discussed in the Λ-hypernuclear production via the K^--atomic capture [19], we may calculate the expression Eq. (21) with n_Ξ arbitrarily chosen, consequently averaging over the l_Ξ distribution $P(l_\Xi)=\Sigma_{n_\Xi}p(n_\Xi,l_\Xi)$. The reason is given as follows: Since Eq. (21) is independent of the normalization of the atomic wave function $\chi_{n_\Xi l_\Xi}$, and also since the amplitudes for the various $\chi_{n_\Xi l_\Xi}$ with a given l_Ξ are, to an excellent approximation, proportional to each other in the target nuclear region, the dependence of the calculated production rates on n_Ξ becomes very small (to be better than 1%).

According to the cascade calculation with $V_{0\Xi}=16$ MeV [11], the Ξ^- particle is mainly absorbed into ^{12}C from the d_Ξ-atomic orbit with the absorption rate of $R_a(d_\Xi)\simeq 87\%$. As for the p_Ξ and f_Ξ absorptions, their contributions are, respectively, $R_a(p_\Xi)\simeq 5\%$ and $R_a(f_\Xi)\simeq 8\%$, while the s_Ξ absorption is as small as $R_a(s_\Xi)\simeq 0.04\%$. When we use $V_{0\Xi}=24$ MeV, the qualitative changes do not occur seriously from the above results. Since the recent KEK-E224 experiment [17] suggests the preference of $V_{0\Xi}=16$ MeV from the analysis of the (K^-,K^+) reaction, we show in Table VIII the calculated production rates per Ξ averaged over the absorption rates of the Ξ^- atom only in the case of $V_{0\Xi}=16$ MeV, where we neglect the contribution from the f_Ξ absorption. The results are almost the same as those given in the $(3d)_\Xi$-atomic capture case (see Sec. IV B), because the Ξ^- particle is mainly absorbed from the d_Ξ orbits. The calculated production rate per Ξ for $^{6}_{\Lambda\Lambda}$He is as small as 0.23%. This is in contrast to the calculated results for the compound double-Λ hypernuclear

picture [9] that the ${}^{6}_{\Lambda\Lambda}$He hypernucleus is produced very much. The KEK-E176 experimental data [2,3] shows no evidence of ${}^{6}_{\Lambda\Lambda}$He, which is consistent with our calculated results. As for the twin-Λ hypernuclear production, the averaged production rate per Ξ^- (R/Ξ^-) for the ${}^{9}_{\Lambda}\mathrm{Be}+{}^{4}_{\Lambda}\mathrm{H}$ channel ($R/\Xi^-=0.07\%$) is about twice larger than that for the ${}^{8}_{\Lambda}\mathrm{Li}+{}^{5}_{\Lambda}\mathrm{He}$ channel ($R/\Xi^-=0.04\%$), and the value of R/Ξ^- for the excited channel ${}^{9}_{\Lambda}\mathrm{Be}(2^+)+{}^{4}_{\Lambda}\mathrm{H}$ is almost the same as that for the ground-state channel ${}^{9}_{\Lambda}\mathrm{Be}(0^+)+{}^{4}_{\Lambda}\mathrm{H}$. The results are consistent with the KEK-E176 experimental results [2,3], namely, that only the ${}^{9}_{\Lambda}\mathrm{Be}+{}^{4}_{\Lambda}\mathrm{H}$ channel is observed (two events), in which one event is ${}^{9}_{\Lambda}\mathrm{Be}(0^+)+{}^{4}_{\Lambda}\mathrm{H}$ and another is ${}^{9}_{\Lambda}\mathrm{Be}(2^+)+{}^{4}_{\Lambda}\mathrm{H}$.

The calculated double-Λ sticking probability, which is defined as the sum of the averaged production rates per Ξ^- for double-Λ hypernuclei (4.7%) and twin-Λ hypernuclei (0.1%), is $P^{\mathrm{cal}}_{\Lambda\Lambda}=4.8\%$ from Table VIII. It seems that the value is not seriously changed for the case of the Ξ^--atomic capture into other light nuclei such as ^{14}N and ^{16}O, since the threshold energies for double-Λ and twin-Λ hypernuclear production channels for Ξ^--atomic systems with light nuclei are not varied drastically in comparison with those for the ${}^{12}\mathrm{C}+\Xi^-$ atomic system as shown in Fig. 1. Therefore, the value of $P_{\Lambda\Lambda}=4.8\%$ may be considered as the typical one for the Ξ^--atomic capture into other light p-shell nuclei. According to the Ξ^- capture experiment at rest into light nuclei in emulsion (C, N, O) [3], the experimental double-Λ sticking probability is about 5–10%, which is in agreement with our value ($P_{\Lambda\Lambda}=4.8\%$). However, our calculated results show that the main component of $P_{\Lambda\Lambda}=4.8\%$ comes from the double-Λ hypernuclear productions, while the KEK-E176 experimental results show that the number for the double-Λ hypernuclear events is only one, and that for the twin-Λ hypernuclear events is only two, of about 30 events of Ξ^- capture at rest into light nuclei in emulsion (C, N, O). (See Sections IV A and IV B for the reason why the double-Λ production rates per Ξ^- are larger than the twin-Λ ones in the present calculation.) Since the difference between our results and experimental results might come from the poor experimental statistic or other production mechanism, we hope that the Ξ^--atomic capture experiment with higher statistics will be performed in the near future.

V. SUMMARY

The production rates per Ξ^- (R/Ξ^-) via the ${}^{12}\mathrm{C}+\Xi^-$-atomic system with the $(2p)_{\Xi}$ and $(3d)_{\Xi}$ orbits have been investigated for the ${}^{12}_{\Lambda\Lambda}\mathrm{Be}+p$, ${}^{12}_{\Lambda\Lambda}\mathrm{B}+n$, ${}^{11}_{\Lambda\Lambda}\mathrm{Be}+d$, ${}^{10}_{\Lambda\Lambda}\mathrm{Be}+t$, ${}^{9}_{\Lambda\Lambda}\mathrm{Li}+\alpha$, ${}^{6}_{\Lambda\Lambda}\mathrm{He}+{}^{7}\mathrm{Li}$, ${}^{5}_{\Lambda\Lambda}\mathrm{H}+{}^{8}\mathrm{Be}$, ${}^{9}_{\Lambda}\mathrm{Be}+{}^{4}_{\Lambda}\mathrm{H}$, ${}^{8}_{\Lambda}\mathrm{Li}+{}^{5}_{\Lambda}\mathrm{He}$, and ${}^{12}_{\Lambda}\mathrm{B}+\Lambda$ channels (including their excited channels) within the frame of the doorway double-Λ hypernuclear picture (direct reaction picture). The picture is based on the following production mechanism: a Ξ^- particle in an atomic orbit or a hypernuclear state interacts with a proton in ^{12}C to produce two Λ particles, and then a highly excited double-Λ hypernuclear state $[{}^{11}\mathrm{B}^*\otimes\Lambda\otimes\Lambda]$ is formed as an intermediate state with the configuration of two Λ particles coupled with the *proton-hole* core, which is fragmented mainly in the doorway stage to double-Λ or single-Λ hypernuclei by emitting some nucleons or clusters. The obtained results are summarized as follows:

(1) The excited channels of ${}^{12}_{\Lambda\Lambda}\mathrm{Be}+p$, ${}^{12}_{\Lambda\Lambda}\mathrm{B}+n$, and ${}^{11}_{\Lambda\Lambda}\mathrm{Be}+d$ are produced more strongly than other channels. The reasons are twofold: One is that the spectroscopic factors for the fragmentation of ^{11}B to the excited channels of ${}^{10}\mathrm{B}+n$, ${}^{10}\mathrm{Be}+p$, and ${}^{9}\mathrm{Be}+d$ are considerably larger than those of their ground-state channels as well as the ${}^{8}\mathrm{Be}+t$ and ${}^{7}\mathrm{Li}+\alpha$ channels. Another reason is that the excited channels of ${}^{12}_{\Lambda\Lambda}\mathrm{Be}+p$, ${}^{12}_{\Lambda\Lambda}\mathrm{B}+n$, and ${}^{11}_{\Lambda\Lambda}\mathrm{Be}+d$ have broad resonancelike states around the ${}^{12}\mathrm{C}+\Xi^-$ threshold because of their small-Q values.

(2) The production rates per Ξ^- depend on the atomic orbital angular momentum of the Ξ^- particle absorbed into nuclei. In the $(3d)_{\Xi}$-atomic capture case, (where the process mainly occurs according to the cascade calculation), the largest and next largest production-rate-per-Ξ^- channels are excited channels, ${}^{11}_{\Lambda\Lambda}\mathrm{Be}(L^{\pi}=2^+_1)+d$ and ${}^{12}_{\Lambda\Lambda}\mathrm{B}^{t=0s=1}(L^{\pi}=1^-_1)+p$, respectively, with $R/\Xi^-=1.68$ and 0.91 %, in which the double-Λ hypernuclear states correspond, respectively, to $[{}^{9}\mathrm{Be}(l^{\pi}=1^-)\otimes s_{\Lambda}\otimes p_{\Lambda}]$ and $[{}^{10}\mathrm{B}^{t=0s=1}(l^{\pi}=0^+)\otimes s_{\Lambda}\otimes p_{\Lambda}]$, which have the nuclear-core states with one Λ particle in the s_{Λ} state and another in p_{Λ}. On the other hand, in the $(2p)_{\Xi}$-atomic capture case, the largest and second largest production-rate-per-Ξ^- channels are excited channels, ${}^{12}_{\Lambda\Lambda}\mathrm{B}^{t=0s=1}(L^{\pi}=2^+_2)+n$ and ${}^{12}_{\Lambda\Lambda}\mathrm{Be}(L^{\pi}=2^+_2)+p$, respectively, with $R/\Xi^-=2.28$ and 2.03 %, in which the double-Λ hypernuclear states correspond, respectively, to $[{}^{10}\mathrm{B}^{t=0s=1}(l^{\pi}=2^+_2)\otimes s_{\Lambda}\otimes s_{\Lambda}]$ and $[{}^{10}\mathrm{Be}(l^{\pi}=2^+_2)\otimes s_{\Lambda}\otimes s_{\Lambda}]$, which have the nuclear-core excited states with both the two Λ particles in the s_{Λ} state.

(3) The reasons why in the $(3d)_{\Xi}$ $[(2p)_{\Xi}]$ atomic capture the double-Λ hypernuclei with the $(s_{\Lambda}p_{\Lambda})$ $[(s_{\Lambda})^2]$ configuration are produced larger than those with $(s_{\Lambda})^2$ $[(s_{\Lambda}p_{\Lambda})]$ are twofold. One reason is given as follows: Owing to the fact that the Ξ^- particle in the atomic state interacts mainly with a $(0p)$ proton in ^{12}C and the ${}^1S_0$-wave-type conversion undergoes for $\Xi^-+p\rightarrow\Lambda+\Lambda$, the two Λ particles produced by the $(2p)_{\Xi}$ $[(3d)_{\Xi}]$ atomic capture reaction should occupy mainly in the $(s_{\Lambda})^2$ $[(s_{\Lambda}p_{\Lambda})]$ configuration due to the parity conservation for the t matrix $\langle\Lambda\Lambda|v_{\Xi^-p\rightarrow\Lambda\Lambda}({}^1S_0)|(2p)_{\Xi}(0p)_{\mathrm{proton}}\rangle$ ($\langle\Lambda\Lambda|v_{\Xi^-p\rightarrow\Lambda\Lambda}({}^1S_0)|(3d)_{\Xi}(0p)_{\mathrm{proton}}\rangle$). This is a selection rule for the double-Λ hypernuclei produced by the Ξ^--atomic capture reaction. Another reason is that the ${}^{11}_{\Lambda\Lambda}\mathrm{Be}+d$ and ${}^{12}_{\Lambda\Lambda}\mathrm{B}+n$ channels with the $(s_{\Lambda}p_{\Lambda})$ configuration [${}^{12}_{\Lambda\Lambda}\mathrm{B}+n$ and ${}^{12}_{\Lambda\Lambda}\mathrm{Be}+p$ with $(s_{\Lambda})^2$] and the total angular momentum with $J^{\pi}=2^+$ (1^-) have broad resonancelike states around the ${}^{12}\mathrm{C}+\Xi^-$ threshold, while those with the $(s_{\Lambda})^2$ configuration [${}^{12}_{\Lambda\Lambda}\mathrm{B}+n$ and ${}^{12}_{\Lambda\Lambda}\mathrm{Be}+p$ with $(s_{\Lambda}p_{\Lambda})$] do not have them.

(4) Since the excited double-Λ hypernuclear states can emit a nucleon or a Λ particle, the following sequential processes are possible: $({}^{12}\mathrm{C},\Xi^-)_{3d\text{-},2p\text{-atom}}\rightarrow{}^{12}_{\Lambda\Lambda}\mathrm{B}^*+n\rightarrow{}^{11}_{\Lambda\Lambda}\mathrm{Be}+p+n$ or ${}^{11}_{\Lambda\Lambda}\mathrm{B}+n+n$, and $({}^{12}\mathrm{C},\Xi^-)_{3d\text{-atom}}\rightarrow{}^{11}_{\Lambda\Lambda}\mathrm{Be}^*+d\rightarrow{}^{10}_{\Lambda\Lambda}\mathrm{Be}+n+d$ or ${}^{10}_{\Lambda}\mathrm{Be}+\Lambda+d$. These processes are similar to the sequential process for the ${}^{13}_{\Lambda\Lambda}\mathrm{B}$ production observed in the KEK-E176 experiment, $({}^{14}\mathrm{N},\Xi^-)_{\mathrm{atom}}\rightarrow{}^{14}_{\Lambda\Lambda}\mathrm{C}^*+n\rightarrow{}^{13}_{\Lambda\Lambda}\mathrm{B}+p+n$.

(5) The calculated production rate per Ξ^- for ${}^{6}_{\Lambda\Lambda}$He is as

small as 0.23%. This is in contrast to the calculated results for the compound double-Λ hypernuclear picture, which predicts a plethora of the ${}^{6}_{\Lambda\Lambda}$He hypernucleus. The KEK-E176 experimental data shows no evidence of ${}^{6}_{\Lambda\Lambda}$He, which is consistent with our calculated results.

(6) As for the twin-Λ hypernuclear production, the production rates per Ξ are smaller than those for the double-Λ hypernuclei. The calculated production rates per Ξ for the ${}^{9}_{\Lambda}\mathrm{Be}+{}^{4}_{\Lambda}\mathrm{H}$ channel ($R/\Xi=0.07\%$) is about twice larger than that for the ${}^{8}_{\Lambda}\mathrm{Li}+{}^{5}_{\Lambda}\mathrm{He}$ channel ($R/\Xi=0.04\%$). We found that the production rate per Ξ for the excited channel ${}^{9}_{\Lambda}\mathrm{Be}(2^{+})+{}^{4}_{\Lambda}\mathrm{H}$ is almost the same as that for the ground-state channel ${}^{9}_{\Lambda}\mathrm{Be}(0^{+})+{}^{4}_{\Lambda}\mathrm{H}$. The results are consistent with the KEK-E176 experimental results that only the ${}^{9}_{\Lambda}\mathrm{Be}+{}^{4}_{\Lambda}\mathrm{H}$ channel has been observed so far (two events), in which one event is ${}^{9}_{\Lambda}\mathrm{Be}(0^{+})+{}^{4}_{\Lambda}\mathrm{H}$ and another is ${}^{9}_{\Lambda}\mathrm{Be}(2^{+})+{}^{4}_{\Lambda}\mathrm{H}$.

(7) The production rate per Ξ for the ${}^{12}_{\Lambda}\mathrm{B}+\Lambda$ channel is comparable to those for the double-Λ hypernuclei. We found that the excited states of ${}^{12}_{\Lambda}\mathrm{B}$ are produced as much as the ground state.

(8) The calculated double-Λ sticking probability, the sum of production rates per Ξ for double-Λ and twin-Λ hypernuclei, is about 5%. This value is in agreement with the KEK-E176 experimental data. However, our calculated results show that the main component of the double-Λ sticking probability comes from the double-Λ hypernuclear production, while the experimental results show that the double-Λ hypernuclear event is only one, and the twin-Λ hypernuclear event is only two, of about 30 events of Ξ^{-} capture at rest into light nuclei in emulsion (C, N, O). The difference between our results and experimental results might come from the poor experimental statistic or other production mechanisms. In order to clarify the production mechanism, it is highly hoped that a Ξ-atomic capture experiment with higher statistics will be performed in the near future.

[1] C. B. Dover and A. Gal, Ann. Phys. (N.Y.) **146**, 309 (1983); H. Bandō, T. Motoba, and J. Žofka, Int. J. Mod. Phys. A **5**, 4021 (1990).

[2] S. Aoki *et al.*, Prog. Theor. Phys. **95**, 1287 (1991).

[3] S. Aoki *et al.*, Prog. Theor. Phys. **89**, 493 (1993); Phys. Lett. B **355**, 45 (1995); K. Nakazawa, Nucl. Phys. **A585**, 75c (1995); *Proceedings of the 23rd INS International Symposium on Nuclear and Particle Physics with Meson Beams in the 1 GeV/c*, edited by S. Sugimoto and O. Hashimoto (Universal Academic, Tokyo, 1995), p. 261.

[4] C. B. Dover, D. J. Millener, A. Gal, and D. H. Davis, Phys. Rev. C **44**, 1905 (1991).

[5] M. Danysz *et al.*, Phys. Rev. Lett. **11**, 20 (1963); Nucl. Phys. **A450**, 311c (1986); R. H. Dalitz *et al.*, Proc. R. Soc. London, Ser. A **426**, 1 (1989).

[6] D. J. Prowse, Phys. Rev. Lett. **17**, 782 (1966).

[7] Y. Yamamoto, H. Takaki, and K. Ikeda, Prog. Theor. Phys. **86**, 876 (1991).

[8] D. Zhu, C. B. Dover, A. Gal, and M. May, Phys. Rev. Lett. **67**, 2268 (1991).

[9] M. Sano, M. Wakai, and Y. Yamamoto, Prog. Theor. Phys. **87**, 957 (1992); Y. Yamamoto, M. Sano, and M. Wakai, Prog. Theor. Phys. Suppl. **117**, 265 (1994).

[10] T. Yamada and K. Ikeda, Nucl. Phys. **A585**, 79c (1995); Few-Body Syst., Suppl. **9**, 281 (1995); *Proceedings of the 23rd INS International Symposium on Nuclear and Particle Physics with Meson Beams in the 1 GeV/c* (Ref. [3]), p. 279.

[11] T. Koike (private communication).

[12] J. P. Elliot, Proc. R. Soc. London **245**, 128 (1958); **245**, 562 (1958); J. P. Elliot and M. Havey, *ibid.* **172**, 557 (1963); M. Havey, Adv. Nucl. Phys. **1**, 67 (1973).

[13] T. Yamada, M. Takahashi, and K. Ikeda, Phys. Rev. C **53**, 752 (1996).

[14] Y. Yamamoto, T. Motoba, H. Himeno, K. Ikeda, and S. Nagata, Prog. Theor. Phys. Suppl. **117**, 361 (1994).

[15] M. M. Nagel, T. A. Rijken, and J. J. de Swart, Phys. Rev. D **12**, 744 (1975); **15**, 2547 (1977); **20**, 1633 (1979).

[16] A. Hasegawa and S. Nagata, Prog. Theor. Phys. **45**, 1786 (1971); Y. Yamamoto, *ibid.* **52**, 471 (1974).

[17] K. Imai *et al.*, KEK experiment E224.

[18] S. Cohen and D. Kurath, Nucl. Phys. **73**, 1 (1965).

[19] A. Gal and L. Klieb, Phys. Rev. C **34**, 956 (1986).